Environmental Science: Atmospheres

ROYAL SOCIETY OF CHEMISTRY

PAPER

View Article Online
View Journal | View Issue

Cite this: *Environ. Sci.: Atmos.*, 2022, **2**, 517

Characterization, sources, and atmospheric transformation of a few key short-lived climate pollutants (SLCPs) at a rural super-site in the Indo-Gangetic Plain (IGP) of India†

Jai Prakash,‡[ab] Harsh Raj Mishra,[a] Kalyan Mitra,[c] Bhilok Chandra,[a] Mattias Hallquist,[ac] Gazala Habib,[b] Geetam Tiwari,[b] Jan B. C. Pettersson,[c] Johan Boman,[ac] Håkan Pleijel[ad] and Ravi Kant Pathak *[ac]

The Indo-Gangetic Plain (IGP) region of India faces some of the most severe air pollution problems on Earth that threaten human health, food security, ecosystems, environmental sustainability, and the climate. The aim of this study is to identify and characterize the sources of key short-lived climate pollutants (SLCPs) – black carbon (BC), brown carbon (BrC), and ozone (O_3) – as well as other pollutants [carbon monoxide (CO) and nitrogen oxides NO_X = NO and NO_2], and interlinked atmospheric processes of their formation and transformation at our long-term air pollution monitoring station in a remote rural IGP site, the Indo-Gangetic Plains Centre for Air Research and Education (IGP-CARE). Because of its location, measurements acquired at IGP-CARE provide otherwise new information on the key SLCPs in the IGP region at a remote and rural location. The year-long measurement data at this remote site provided new insights into the variability of SLCP concentration and interlinked atmospheric processes that affect air quality in the rural IGP region. Thirteen episodic events (E1–E13) of elevated BC and BrC concentrations were identified, which can largely be attributed to the local biomass burning activities in the neighboring rural communities. It is suggested that high concentrations of BrC were mostly primary in nature and thought to be co-emitted with BC from biomass burning. Also, secondary pollutant tropospheric O_3 showed elevated concentration. O_3 peaks were mostly attributed to local ozone formation. Nevertheless, on several occasions, O_3 emission was also attributed to regional urban areas. This study's most important finding is that BrC concentrations were relatively high throughout the year with very pronounced diurnal variation with distinct morning and evening peaks in general and a minimum at around noon time; this is hypothesized to be associated with daytime photochemical processes. Analyses using a conditional bivariate probability function (CBPF) and potential source contribution function (PSCF) suggest that regional sources likely affected the local concentrations of SLCPs. These results partly explain the high concentrations and spatial distributions of SLCPs at the local and regional scales at the IGP-CARE site in winter and autumn. In contrast, in the summer and monsoon seasons, strong convection likely favored the dilution of pollutants.

Received 17th October 2021
Accepted 4th April 2022

DOI: 10.1039/d1ea00083g

rsc.li/esatmospheres

Environmental significance

Air pollution by short-lived climate pollutants (SLCPs) such as black carbon, brown carbon, and ozone poses a severe threat to human health and food security and may exacerbate problems caused by global climate change. India's Indo-Gangetic Plain (IGP) region has one of the world's highest air pollution burdens, but data on seasonal trends in SLCP levels in this region and their dependence on meteorological factors, atmospheric chemistry, and local and regional emission sources is lacking. This work is significant to atmospheric science because it presents a large set of measurements of atmospheric SLCP concentrations and related factors in the rural IGP region over the course of a year and clarifies their sensitivity to various emission sources and atmospheric processes.

[a]*Indo Gangetic Plains–Centre for Air Research and Education, RuriPara, Hamirpur, UP, India*

[b]*Department of Civil Engineering, Indian Institute of Technology Delhi, New Delhi-110016, India*

[c]*Atmospheric Science, Department of Chemistry and Molecular Biology, University of Gothenburg, SE-41296 Gothenburg, Sweden. E-mail: ravikant@chem.gu.se; Tel: +46-766229095*

[d]*Department of Biological and Environmental Science, University of Gothenburg, SE-41296 Gothenburg, Sweden*

† Electronic supplementary information (ESI) available. See https://doi.org/10.1039/d1ea00083g

‡ Independent Researcher: New Delhi, 110016, India.

1. Introduction

Short-lived climate pollutants (SLCPs) have shorter lifetimes in the atmosphere than greenhouse gases (GHGs) but have important effects on climate change and human health.[1,2] SLCPs include atmospheric aerosols containing black carbon (BC), organic carbon (OC), sulfate, and nitrate, and gases including tropospheric ozone (O_3), methane (CH_4), carbon monoxide (CO), nitrogen oxides (NO_X), sulfur dioxide (SO_2), and hydrofluorocarbons (HFCs).[3] BC, O_3, and CH_4 cause warming of the atmosphere whereas OC enhances atmospheric cooling. Among the SLCPs, BC (a component of soot) is produced by incomplete combustion of fossil fuels, solid biomass fuels, and agricultural residues, which absorb sunlight and warm the atmosphere. In addition, BC affects the radiative properties of both clouds and snow/ice cover.[4,5] More recently, a fraction of organic aerosols has been termed "brown carbon (BrC)", which also absorbs light more strongly, and is a plausible cause of radiative effects on the energy balance.[6–9] BrC is co-emitted with BC from the combustion of biomass and fossil fuels and also, it is considered as a component of secondary organic aerosols (SOA). Thus, BrC originates from both primary and secondary sources; it comprises emissions from biomass burning. BrC has a wide range of physicochemical and optical properties that are difficult to be generalized,[10,11] and also includes water-soluble organic compounds (WSOC).[12,13] In the atmospheric aerosol, some fraction composed of mineral dust can also weakly absorb light.[13]

Another potent SLCP, tropospheric O_3, is a typical secondary pollutant in the atmosphere and poses a serious threat to human health[14–16] and vegetation.[17,18] BC and co-emitted species undergo a variety of photochemical transformations that increase tropospheric O_3 and SOA.[19,20] However, BC interacts with O_3 precursors (*e.g.* CO, NO_X, and non-methane volatile organic compounds (NMVOCs)), and increases BC absorption under favorable meteorological conditions.[5,21]

The IGP region of India harbors a population of about 750 million,[22,23] many of whom burn residential biomass to meet some of their daily energy needs. Open biomass burning is one of the major sources of BrC,[24] and it is also expected in rural parts of the IGP of India. Approximately 80% of rural households in the IGP region use unprocessed solid biomass fuel such as wood, dung cakes, and agricultural residues for domestic cooking and space heating.[25–27]

Consequently, it is a major "global hotspot" of biomass burning and SLCP production, which results in the formation of atmospheric brown clouds (ABC).[4,28,29] In winter, the persistent ABC over the IGP region has a remarkably high content of key SLCPs and has significant adverse effects on regional air quality, climate, human health, and food security.[16,29,30] The levels of these key SLCPs appear to originate from open biomass burning, on-road transport, domestic burning, industrial sites, brick kilns, and crop waste burning. These SLCPs can be transported over long distances, and they can adversely affect otherwise pristine areas with low levels of SLCP production, depending on the wind speed and direction. Previous studies have shown that during a 5 month period (November to March) extending from late autumn to early spring, large quantities of SLCPs accumulate over the IGP region[31–34] and Central Himalayas.[35–37] Several studies on SLCPs including BC and O_3 have been previously reported for urban regions of the IGP, *e.g.* Delhi, Kanpur, Varanasi, *etc.*[38–40] Few short-term studies in rural IGP or remote areas showed significant variability in BC and BrC concentrations.[41,42] The BC optical properties and morphology can be significantly altered through condensation of SOA on BC.[4,43,44] These studies outlined that BC light absorption enhancement can contribute to the higher warming potential of the BC.[4,44,45] Due to the diversity of potential SLCP precursors, rural anthropogenic activities, and the complexity of atmospheric chemistry, there persist knowledge gaps about the long term atmospheric evolution and transformations of BC, BrC and O_3 in rural areas of the IGP. Therefore, long-term measurements are needed to elucidate the formation, transformation, and variation in concentration of BC and BrC, O_3, and SOA as well as the chemical processes connecting these species. However, very few long-term measurement/observation campaigns have been previously conducted in the rural IGP region. To address this gap, we established IGP-CARE, the first dedicated long-term atmospheric pollution measurement station in the rural IGP. Here we present measurements of key SLCPs including BC, BrC, and ozone precursors, and analyze their seasonal and intra-annual variations to identify the atmospheric processes and chemical reactions governing the evolution of SLCP levels. We also investigate the transformation of BrC and it provided insights into the impact of meteorological factors on SLCPs.

2. Materials and methods

2.1 Site descriptions and real-time instruments

To facilitate long-term measurement of SLCPs in the IGP region, a new monitoring site was established in 2016 in a rural area. This site, the Indo-Gangetic Plains Centre for Air Research and Education (IGP-CARE), is situated in agricultural fields adjacent to a forest by the River Burma (a tributary of the River Betwa) surrounded by six villages in the Hamirpur district of Uttar Pradesh (25° 48′ 55.5″ N; 79° 55′ 07.5″ E), India (see Fig. 1). The major sources of BC and other co-pollutants near this rural site are burning of solid biofuels (*e.g.* wood and dung cakes) and agricultural residues for domestic cooking and space heating. The study site is remote/rural and therefore, there are no major sources of fossil fuel combustion such as DG sets/vehicles/wick lamps nearby. The nearest roadside/highway (SH-42) is approximately 10 km away from the IGP-CARE station. Therefore, this rural site has insignificant emissions from combustion of fossil fuels such as coal, diesel, and gasoline as compared to other locations of the IGP region.

Real-time long-term measurements of SLCPs have been conducted continuously at the IGP-CARE site since January 2017. The dataset examined in this study covers the period from January 2017 to December 2017. Ecotech analyzers (ACOEM Group, Melbourne, Australia) were used to measure O_3 (Serinus® 10 model), NO_X (Serinus® 40 model), and CO

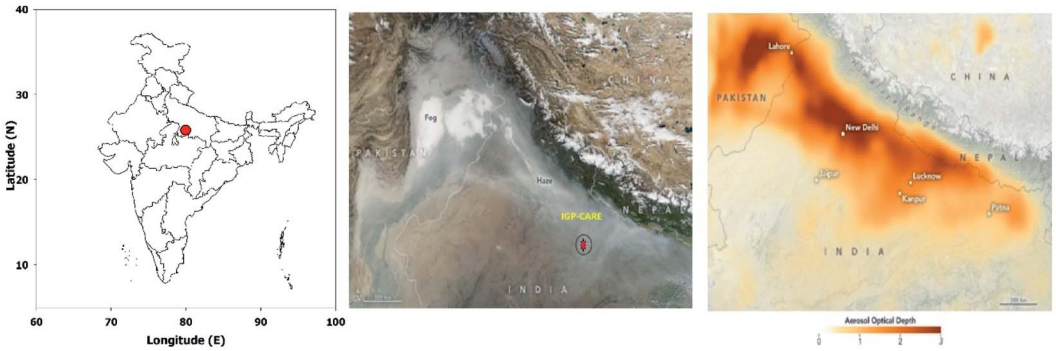

Fig. 1 The rural Indo-Gangetic Plains Centre for Air Research and Education (IGP-CARE) monitoring station (red circle) in the IGP region, Hamirpur, India (left panel). A satellite view of haze spread over the IGP region, India, and the IGP-CARE location (middle panel), and a view of the AOD (right panel) over the IGP region (source: https://earthdata.nasa.gov/).

(Serinus® 30 model). BC and UV-absorbing particulate matter (UVPM) were determined with a black carbon monitor (BC 1050 series, Met One Instruments, Inc., Washington, USA) on quartz filter tape at two wavelengths (375 and 880 nm). BC absorbs light at 880 nm, while UVPM is measured at 375 nm. Since the IGP-CARE site is remote and very far from mineral dust sources, *e.g.* deserts (the nearest desert (Thar desert) is 1000^{+} km away), the probability for contribution of other light absorption components such as mineral dust to the UVPM fraction of $PM_{2.5}$ is minimal for several reasons: (a) the mass absorption efficiency (MAE) of mineral dust (0.095–0.711 $m^2\ g^{-1}$)[46] is significantly smaller than that of BrC from biomass burning (0.51–5.0 $m^2\ g^{-1}$);[44,47] (b) a large fraction of mineral dust is in the coarse mode in northern India;[48] (c) the IGP-CARE site is remote and rural, surrounded by small villages where biomass burning is the main activity for cooking and heating around the year and hence carbonaceous aerosols are thought to be significantly dominant in fine particles. The difference between the concentrations of UVPM and BC provides an estimate of the BrC concentration and is henceforth referred to simply as BrC in this paper.[49,50] Meteorological parameters such as the temperature, pressure, relative humidity, wind speed, and wind direction at the site were monitored using an Automatic Weather Station (AWS) (Davis Vantage Pro 2, Davis Instruments Corporation, USA) during the sampling period. All instrument inlets were mounted 20 m above the ground surface. ESI Table S1† lists the instruments used to measure SLCPs at IGP-CARE together with their minimum detection limits (MDLs) and the measurement time intervals. For quality assurance (QA) and quality control (QC) purposes, instruments were calibrated every 30 days during the sampling period, as specified by their manufacturers. The calibration process included flow calibration and leakage tests. Solar power generation was used exclusively to avoid potential local emission biases at the IGP-CARE site.

2.2 Data processing

High resolution (~1 minute) data was obtained with each instrument used at IGP-CARE. Spurious values [not available (NA), negative, and zero] were removed from the dataset prior to further analysis. All datapoints relating to SLCPs were averaged over 1 h windows to ensure consistency of datapoints from different instruments. The seasons at the IGP-CARE site were defined in accordance with the practices of the Indian Meteorological Department (IMD): winter (December, January, and February), summer (March, April, May, and June), monsoon (July, August, and September), and autumn (October and November). Fire products were obtained from the Visible Infrared Imaging Radiometer Suite (VIIRS) and Suomi National Polar-orbiting Partnership (SNPP) [VIIRS S-NPP] for the region where IGP-CARE is located (25°N to 28°N and 79°E to 82°E) during the year 2017. Detailed information on fire products can be obtained from the Fire Information for Resource Management System (FIRMS) website (https://firms.modaps.eosdis.nasa.gov/). To obtain the planetary boundary layer height (PBLH), we retrieved hourly PBLH data for the IGP-CARE region from the European Centre for Medium-Range Weather Forecasts (ECMWF) reanalysis dataset, ERA-Interim.[51]

To compensate for the filter loading effect of BC, we used the algorithm developed by Virkkula *et al.* in 2007 (ref. 52) to correct for light attenuation (ATN, defined as the ratio of incoming to outgoing light intensities before and after passage through a filter) in the black carbon analyzer. Different approaches are used for the correction of loading and multiple-scattering effects in filter-based instruments.[52–57] It should be noted that a multiple scattering correction algorithm has been introduced by Coen *et al.* (2010)[56] and Kim *et al.* (2019)[57] based on scattering measurements using instruments such as a nephelometer, photo-acoustic spectrometer or multi-angle absorption platform. Despite such corrections, inter-comparability of different instruments for the determination of the aerosol absorption properties is still an open methodological issue, especially for ambient aerosol measurements. In this study, the scope of multiple scattering corrections was limited due to unavailability of simultaneous measurements of the scattering from the deposited particle on the filter type of our instrument: BC monitor – BC1050 (Met One Inc., USA). Therefore, a widely popular method given by Virkkula *et al.* (2007)[52] for correction of light attenuation was thought to be more suitable for our

measurements. Also, this correction method has been widely used by studies for BC measurement and their filter loading correction in the IGP region and other parts of India.[58] The correction was performed using the following equation.

$$BC_{corrected} = (1 + k \times ATN) \times BC_{uncorrected} \quad (1)$$

Here, ATN is the attenuation value after a filter change or filter advancement and k is an empirical term whose value is obtained using the following equation:

$$BC_{corrected}\ (t_{i,last}) = BC_{corrected}\ (t_{i+1,last}) \quad (2)$$

Here, $BC_{corrected}\ (t_{i,last})$ is the last corrected BC value for the old filter spot and $BC_{corrected}\ (t_{i+1,last})$ is the first corrected BC value for the new filter spot. Using eqn (2), eqn (1) can be rewritten to estimate k:

$$k_i = \frac{BC_{uncorrected}\ (t_{i+1,last}) - BC_{uncorrected}\ (t_{i,last})}{ATN(t_{i,last}) \times BC_{uncorrected}\ (t_{i,last}) - ATN(t_{i+1,last}) \times BC_{uncorrected}\ (t_{i+1,last})} \quad (3)$$

If the filter location is changed, the ATN value becomes 0, and eqn (3) simplifies to:

$$k_i \approx \frac{1}{ATN(t_{i,last})}\left(\frac{BC_{uncorrected}\ (t_{i+1,last})}{BC_{uncorrected}\ (t_{i,last})} - 1\right) \quad (4)$$

The k_i term is used to correct data acquired at filter location i according to eqn (1). However, ATN is rarely exactly 0 even for the first measurements at a new location. The final measurements for filter location i and the first three for filter spot $i + 1$ were therefore acquired with a temporal resolution of 1 minute.

Statistical analyses were performed using RStudio (R Development Core Team, 2015), taking advantage of packages including 'openair', 'ggplot2', 'dplyr', and 'tidyverse'. Probability functions based on a conditional bivariate probability function (CBPF) and a potential source contribution function (PSCF) were evaluated for the purpose of locating local and regional SLCP sources. More details of the CBPF and PSCF analyses are presented in Text S1 and S2 of the ESI.† These functions were implemented using the openair R package.[59,60]

3. Results and discussion

3.1 Statistical summary

Statistical summaries of the key SLCP levels and meteorological parameters measured over 365 days (January 2017 to December 2017) during the study period are presented in Table 1. During this period, the BC concentration ranged from 2.1 to 16.6 μg m^{-3} with an overall mean of 5.1 ± 2.2 μg m^{-3}, while the BrC concentration ranged from 0.5 to 32.3 μg m^{-3} with an overall mean of 2.6 ± 1.3 μg m^{-3}. The overall mean concentrations of O_3, CO, and NO_X were (31.0 ± 23.1) ppbv, (659 ± 437) ppbv, and (8.6 ± 3.5) ppbv, respectively.

The summary statistics of SLCPs and meteorological parameters measured during the day and night in 2017 over IGP-CARE are presented in Table S2† of the ESI. For BC, BrC, and CO, the night-time means and median concentrations were higher than the corresponding day-time means and medians. However, the reverse was true for O_3 and NO_X

Table 1 Summary statistics of SLCPs and meteorological parameters measured over IGP-CARE during the year 2017

Variable	Min.	Max.	Median	Mean	SD	*N*
Short-lived climate pollutants (SLCPs)						
BC (μg m^{-3})	2.1	16.6	4.7	5.1	2.2	7974
BrC (μg m^{-3})	0.5	32.3	2.5	2.6	1.3	7974
O_3 (ppbv)	0.2	207.3	26.4	31.0	23.1	7956
CO (ppbv)	17.0	3351	791	659	437	4566
NO (ppbv)	0.0	2.7	0.1	0.4	0.3	5987
NO_2 (ppbv)	1.2	22.1	5.9	9.0	3.7	5987
NO_X (ppbv)	1.1	20.8	5.7	8.6	3.5	5987
BrC/BC ratio	0.0	13.7	0.5	0.5	0.3	7443
CO/NO_X ratio	0.1	500.0	73.0	87.2	72.6	3930
NO_X/BC ratio	0.3	73.7	1.74	2.26	1.93	5168
Meteorological parameters						
Temperature (°C)	7.4	46.3	27.5	26.5	7.7	8067
Relative humidity (%)	7.5	100.0	65.5	63.3	21.0	8067
Wind speed (m s^{-1})	0.0	12.5	1.3	1.8	1.8	8067
Solar radiation (W m^{-2})	67.4	686.3	29.5	77.2	107.2	8067
Planetary boundary layer height (m)	11.0	4878	209	603	832	8755

concentrations. The mean concentrations were higher than the corresponding medians, indicating the occurrence of periodic high concentration events due to meteorological parameters in specific seasons, and therefore, correlations among these key SLCPs and meteorological parameters in different seasons were investigated by conducting pairwise Pearson correlation and are depicted in Fig. S1† in the ESI and discussed further below.

During the study period, the temperature ranged from 7.4 °C to 46.3 °C with a mean of 26.5 °C, the RH ranged from 7.4 to 100.0% with a mean of 63.3%, and the wind speed ranged from 0 to 12.5 m s^{-1} with mean of 1.8 m s^{-1} (see Table 1). The daily variation in the meteorological parameters and wind roses at IGP-CARE are shown in Fig. S2† of the ESI. Winters in the IGP region are generally cold with temperatures ranging from 7.8 °C to 34.2 °C (17.2 ± 4.8 °C) and moderate to high humidity (72 ± 16%) with low wind speeds (1.0 ± 0.8 m s^{-1}) and low PBLH (422 ± 320 m); however, the IGP region becomes very hot in summer with high temperature (31.4 ± 6.5 °C), low RH (46 ± 18%), high PBLH (1196 ± 929 m) and high wind speed (4.7 ± 1.8 m s^{-1}). In the monsoon season, the IGP-CARE site was observed to have moderate temperature (29.7 ± 2.8 °C) and high RH (80 ± 12%) with low PBLH (481 ± 375 m). The measured wind direction oscillated between north-east (NE) and south-west (SW) over the entire study period (Fig. S2b†); the wind was predominantly easterly during winter, while during summer the wind direction was mainly easterly and southeasterly. In monsoon months, the prevailing wind direction changed from north-east to south-west (SW); this is typical for the Indian monsoon season and is due to a region of high pressure over the Indian ocean that causes heavy rainfall. At the end of the autumn months, the wind direction began shifting back to north-east (NE) (Fig. S2c†). The SLCP concentration is affected by meteorological parameters, and co-founding factors such as geographical region, emission sources, *etc.* However, variations of temperature, RH, PBLH, and wind patterns with SLCP levels are discussed in further sections.

3.2 Correlation analysis between SLCPs and meteorological parameters

The Pearson correlation among key SLCPs and meteorological parameters is depicted in Fig. S1† in the ESI during the study period of IGP-CARE. The hourly concentrations of BC were positively well correlated in all seasons except monsoon with the hourly concentrations of BrC ($r^2 = 0.61$ in autumn; $r^2 = 0.56$ in summer; $r^2 = 0.52$ in winter; and $r^2 = 0.32$ in monsoon). Both BC and BrC had moderate to high association with CO in winter and autumn seasons, while a relatively poor correlation was observed in other seasons. This is an indication of similar sources of emission of BC, BrC, and CO, such as biomass burning in autumn and winter and local burning (mud-brick firing, crop residue burning, *etc.*) in summer. Notably, negative and weak correlations existed between O_3 and NO_2 ($r^2 = -0.03$ in winter; $r^2 = -0.15$ in summer; $r^2 = -0.07$ in monsoon; and $r^2 = -0.25$ in autumn). Both BC and BrC had moderate and positive association with NO_2 in the autumn season and poor but consistent correlation in the winter and summer seasons. Furthermore, moderate and positive correlation was observed between NO_2 and CO in autumn, while poor correlations were noted in other seasons.

In IGP-CARE, the concentrations of BC were moderately well correlated with temperature (TEMP) in all seasons except monsoon ($r^2 = -0.32$ in winter; $r^2 = -0.51$ in summer; $r^2 = -0.42$ in autumn; $r^2 = -0.09$ in monsoon). Compared to BC, moderate and negative correlations between BrC and TEMP ($r^2 = -0.40$ in winter; $r^2 = -0.46$ in summer; $r^2 = -0.39$ in monsoon; and $r^2 = -0.64$ in autumn) were observed. A weak and negative correlation of BC and BrC also existed with TEMP, SR, and WS, which suggests the possibility of a decrease in the BC and BrC in the presence of solar radiation, temperature, and wind speed. Furthermore, moderate and positive correlations were observed between BC, BrC, and RH in winter, summer, and autumn, while weak and negative correlations were noted in monsoon. A moderate to high association was observed between O_3 and TEMP in all seasons in IGP-CARE (Fig. S2† in the ESI), while moderate correlations were observed between O_3 and SR ($r^2 = 0.52$ in winter; $r^2 = 0.48$ in summer), and poor correlations were noted in monsoon ($r^2 = 0.15$) and autumn ($r^2 = 0.27$). Among seasons, negative and weak correlations between TEMP and other key SLCPs (CO, NO, and NO_2) were observed, while other meteorological parameters (SW, SR, and RH) did not have any strong correlation with other key SLCPs.

3.3 Temporal trends of BC and BrC

To outline the sources, characteristics, and processes of SLCPs at the IGP-CARE site, we selected multiple episodic events for further investigation. It should be noted that we consider a holistic interpretation from individual episodes to draw general inferences of SLCP characteristics in IGP-CARE over the study period. BC and co-emitted species are primary pollutants, while O_3 is a secondary pollutant. Thus, they naturally exhibited different pollution episodic characteristics. Therefore, we have presented the observation of high concentration of these pollutants during our measurements in different sections, which are presented in Tables 2 and 3.

Time series plots of the hourly and daily mean variation of BC (top panel), BrC (middle panel), and fire counts (bottom panel) are shown in Fig. 2, which also highlights thirteen episodic events using green shading. Episodic events (E1 to E13) were defined as events during which the BC and BrC concentrations were at least three times the hourly mean (3 × hourly mean) for the study period (see Table S3† in the ESI). The episodic hourly mean BC and BrC levels along with the corresponding BrC/BC ratios, atmospheric process data, and their physical interpretations are summarized in Table 2. The BrC/BC ratio in the atmosphere signifies the abundance of BrC relative to BC, types of emission sources, and atmospheric formation and transformation of organic aerosols. In this study, a higher (larger than the annual hourly mean) BrC/BC ratio is used as an indicator of biomass burning, while a lower BrC/BC ratio (less

Table 2 Concentrations of BC and BrC and their characteristics and interlinked atmospheric processes during episodic events at IGP-CARE

Episodic events	Conc. (μg m^{-3}) mean (median)	Characteristics of pollutants	Atmospheric processes	Interpretation
E1 (7 Jan 2017)	BC 8.5 (9.3) BrC 4.0 (4.3) BrC/BC 0.4 (0.5)	High peaks of BC and BrC, moderate BrC/BC ratio, and no fire counts Very good BC & BrC correlation ($r^2 = 0.96$) at day time, but poor $r^2 = 0.16$ due to meteorological complexity	Calm wind, low mixing height (or PBLH), and low ventilation coefficient (VC), RH ≤ 90%, T ≤ 15 °C, and WD = 115 (E)	High BC and moderate BrC concentrations in the evening due to local biomass burning for cooking and heating purposes, Br/BC ratio decreased initially due to dilution linked to dispersion of local pollutants, then at higher RH the BrC/BC ratio increased indicating local contributions
E2 (12–19 Jan 2017)	BC 6.7 (6.4) BrC 5.7 (6.2) BrC/BC 0.8 (0.8)	High peaks of BrC and BC, high BrC/BC ratio, 4–8 daily fire counts Generally very good BC & BrC correlation on all days ($0.32 < r^2 < 0.96$)	Calm wind, and low PBLH and VC which favour partitioning of organics to the aerosol phase, RH ≤ 74%, T ≤ 14 °C, and WD = 133 (SE)	High BC and BrC levels dominate during the night and evening indicating local biomass burning, high BrC/BC ratio indicates biomass burning with smouldering or high moisture content in the biomass
E3 (21–23 Jan 2017)	BC 5.5 (4.9) BrC 4.4 (3.6) BrC/BC 0.7 (0.8)	High peaks of BC and BrC, and high BrC/BC ratio, 3–4 fire counts Generally very good BC & BrC correlation on all days ($0.51 < r^2 < 0.96$); CO well correlated with BC & BrC	Calm wind, low PBLH, and low VC RH ≤ 70%, T ≤ 18 °C, and WD = 160 (S) Slow dispersion and dilution of BB plumes	Well correlated high BC, BrC and CO levels indicate local biomass burning for cooking/heating and further high BrC/BC ratio indicates plausible moist biomass burning with smoldering
E4 (2–5 Feb 2017)	BC 5.4 (5.5) BrC 2.4 (2.4) BrC/BC 0.4 (0.4)	High peaks of BC, low BrC, moderate BrC/BC ratio, and 4–6 fire counts Generally very good BC & BrC correlation on all days ($0.75 < r^2 < 0.91$); CO well correlated with BC & BrC	Calm wind, low PBLH, and low VC, RH ≤ 76%, T ≤ 19 °C, and WD = 134 (SE)	Night and morning peaks of BC, and moderate BrC/BC ratio indicate local sources of dry biomass burning for cooking
E5 (13–17 Feb 2017)	BC 5.8 (5.5) BrC 2.6 (2.5) BrC/BC 0.4 (0.4)	High peaks of BC, low BrC, moderate BrC/BC ratio, 6–8 fire counts Most days good BC & BrC correlation ($0.25 < r^2 < 0.86$)	Moderate wind and low PBLH and VC, RH ≤ 70%, T ≤ 20 °C, WD = 145 (S)	Night BC levels indicate regional biomass burning from north-IGP with moderate BrC and BC correlation with CO and evening and morning BC peaks indicate local burning for cooking
E6 (9–10 Mar 2017)	BC 4.7 (4.4) BrC 1.8 (1.6) BrC/BC 0.4 (0.4)	High peaks of BC, low BrC, moderate BrC/BC ratio, 5–7 fire counts Most days good BC & BrC correlation ($0.44 < r^2 < 0.87$)	High wind, PBLH and VC (~630 m and 849 m s^{-1}), RH ≤ 70%, T ≤ 21 °C, and WD = 110 (E)	Evening and morning BC and BrC peaks show local burning for cooking
E7 (15–17 Apr 2017)	BC 6.2 (5.7) BrC 1.5 (1.4) BrC/BC 0.2 (0.2)	High BC, low BrC and BrC/BC ratio, and high fire counts (7–10) Mostly good BC & BrC correlation ($0.28 < r^2 < 0.85$)	Moderate wind, PBLH and VC (~881 m and 485 m s^{-1}), RH ≤ 55%, T ≤ 32 °C, and WD = 139 (SE)	Morning and evening BC peaks show local burning for cooking
E8 (20–22 May 2017)	BC 2.0 (1.8) BrC 2.5 (1.2) BrC/BC 1.0 (0.6)	Low BC and BrC levels, high BrC/BC ratio, and 3–4 fire counts Mostly good BC *vs.* BrC correlation ($0.23 < r^2 < 0.77$); CO was well correlated with BC and BrC	High wind, PBLH and VC (~977 m and 2429 m s^{-1}), RH ≤ 32%, T ≤ 36 °C, and WD = 231 (W)	High BrC peak in the night and morning, and odd time high Br/BC ratio indicates local brick firing with biomass burning and smoldering type burning processes; the source of BC, BrC and CO is local biomass burning
E9 (18–19 Oct 2017)	BC 6.0 (5.6) BrC 2.4 (2.4)	High peaks of BC, low BrC, moderate BrC/BC ratio, and 5–7 fire counts	High wind, moderate PBLH (~610 m), and high VC	Night and morning peaks of BC and moderate BrC/BC ratio indicate local biomass burning

Table 2 (*Contd.*)

Episodic events	Conc. (μg m^{-3}) mean (median)	Characteristics of pollutants	Atmospheric processes	Interpretation
	BrC/BC 0.4 (0.4)	Mostly good BC *vs.* BrC correlation ($0.81 < r^2 < 0.89$); CO was also well correlated with BC and BrC	(~3367 m s^{-1}), RH ≤ 58%, $T \leq$ 28 °C, and WD = 123 (E)	(likely dry biomass) at warmer temperatures
E10 (10–11 Nov 2017)	BC 9.5 (9.8) BrC 2.9 (3.0)	High peaks of BC, low BrC, low BrC/BC ratio, and 4–6 fire counts	High wind, moderate PBLH (~410 m), and high VC (~1277 m s^{-1}), RH ≤ 81%, $T \leq$ 21 °C, and WD = 203 (SW)	Afternoon high BC level and high dispersion indicate regional biomass burning from north IGP, and plausible contributions from urban transport (see the time series of SLCP concentrations for the 10–11 Nov. 2017 event in Fig. S7)
	BrC/BC 0.3 (0.3)	Poor BC & BrC correlation ($0.13 < r^2 < 0.26$), but well correlated at night time; CO well correlated with BC and BrC		
E11 (17–20 Nov 2017)	BC 5.9 (5.5) BrC 4.6 (4.6)	High BC, moderate BrC, high BrC/BC ratio, and 5–7 fire counts	High wind, moderate PBLH (~430 m), and high VC (~1767 m s^{-1}), RH ≤ 65%, $T \leq$ 22 °C, and WD = 243 (W)	Moderate levels of BC and BrC, and high BrC/BC indicate local moist biomass with smoldering type burning
	BrC/BC 0.8 (0.8)	Mostly very good BC & BrC correlation ($0.56 < r^2 < 0.89$)		
E12 (4–5 Dec 2017)	BC 6.8 (6.9) BrC 3.9 (4.3)	High BC, moderate BrC, high BrC/BC ratio, and low fire counts (2–3); good BC & BrC correlation ($0.37 < r^2 < 0.75$)	Moderate wind, low PBLH (~300 m), and moderate VC (~1151 m s^{-1}), RH ≤ 64%, $T \leq$ 18 °C, and WD = 210 (SW)	Morning and evening peaks of BC indicate local biomass burning for cooking and heating
	BrC/BC 0.6 (0.6)			
E13 (19–21 Dec 2017)	BC 9.3 (9.3) BrC 2.9 (2.6)	High BC, low BrC, low BrC/BC ratio, and 2–3 fire counts	Low wind, low PBLH (~240 m), and moderate VC (~285 m s^{-1}), RH ≤ 79%, $T \leq$ 16 °C, and WD = 207 (SW)	High BC, low BrC and low BrC/BC ratio indicate contributions from regional urban pollution mixed with local dry biomass burning sources
	BrC/BC 0.3 (0.3)	Mostly poor BC & BrC ($0.04 < r^2 < 0.16$); CO well correlated with BC and BrC		

than the annual hourly mean) is hypothesized to be contributed from non-local sources and atmospheric transformation of organic aerosols. In addition, some studies have used the BrC/BC ratio to identify dominant contributions from biomass burning and other fossil fuel combustion sources.[61–64] Fig. S3† shows the diel variations of these quantities and the ventilation coefficient (VC = PBLH × WS), which is sometimes used as an indicator of the capacity for dilution of pollutants *via* atmospheric processes, during the episodic events.[65]

Episodic event E1 was characterized by high BC and moderate BrC levels (hourly mean of BC and BrC concentrations: 8.5 μg m^{-3} and 4.0 μg m^{-3}, respectively), with a moderate BrC/BC ratio (0.5). During this event, the BC and BrC were elevated in the evening due to burning of solid fuel (wood, dung cakes, and agricultural residues) for cooking and space heating purposes; however, morning BC and BrC datasets of E1 were not captured due to electric power failures. Interestingly, the BC concentrations were strongly associated with BrC (correlation coefficient: 0.86; see Fig. S4† in the ESI), indicating that they probably originated from the same source. As described previously, the IGP-CARE site is remote and rural, surrounded by small villages that burn biomass for their daily needs.

Levels of both BC and BrC during the winter episodes E2 and E3 were higher than those in the rest of the sampling period. In addition, the diel pattern shows that BC, BrC, and BrC/BC ratios were high during the morning and evening time (see Fig S3† in the ESI). Also, there were good correlations between BC and BrC for most days during the events ($0.32 < r^2 < 0.96$ and $0.54 < r^2 < 0.96$) for episodes E2 and E3, respectively (see Fig S4 and Table S4† in the ESI). It is also noted that BC and BrC originated from a similar source.[19,62,66] The high BrC/BC ratios and good correlation of BC and BrC with CO during night-time (see Table S5† in the ESI) in these episodes also corroborate biomass burning as a potent source of BrC and BC. The poor association between BrC and fire radiative power (FRP) for episodes E2 and E3 indicates that BrC was plausibly emitted from the local sources (see Fig S5† in the ESI). It is also noted that this rural site is 10 km away from the nearest roadside and there is no such impact of fossil fuel sources such as DG sets and vehicle emissions.[67]

The episodes (E4 to E7) were characterized by high BC, moderate to low BrC, and high fire counts, with low to moderate BrC/BC ratios (Fig. 2 and Table 2). The moderate correlation between FRP and BrC was observed for the episodes E4 to E6 (Fig. S5† in the ESI). The wind speed and VC were moderate to high during these events and the RH was moderate (55–73%), while high BC levels and low BrC/BC ratios were observed at night, suggesting that partitioning to aerosol was insignificant (Fig S3† in the ESI and Table 2). Also, the hourly NO_X concentrations in episodes E5 and E6 were highly correlated with BC (r^2 = 0.70 and 0.67 in E5 and E6; see Fig S6† in the ESI), which suggests that high wind and PBLH favor the transportation of BC and NO_X emission sources such as agricultural residues burning from regional states, which also mix with local sources such as biomass burning, leading to increased levels of

Table 3 Concentrations of O_3, CO, and NO_X and their characteristics and interlinked atmospheric processes during episodic events at the IGP-CARE

Episodic events	Conc. (ppbv) mean (median)	Pollutant characteristics	Atmospheric processes	Interpretation
I (11–15 Jan)	O_3 – 35.0 (33.0)	Low O_3 and high peaks of CO and NO_X during the morning and evening	Low wind, and low PBLH and VC favour slow dispersion of pollutants that originated from local biomass burning	VC favours slow dispersion of CO that originated from local biomass burning with NO_X
	CO – 636 (568)		RH ≤ 67%, $T \leq 13$ °C, WD = 154 (S)	
	NO_X – 9.6 (9.3)			
II (28 Jan–1 Feb)	O_3 – 27.4 (24.5)	Low peaks of O_3, and high CO and NO_X during the afternoon and evening	Low wind, and low PBLH and VC favour slow dispersion of pollutants that originated from local biomass burning	High variation of CO and NO_X in the afternoon due to local sources such as biomass burning and brick firing processes
	CO – 1041 (1098)		RH ≤ 85%, $T \leq 17$ °C, WD = 141 (SE)	
	NO_X – 9.3 (8.5)			
III (6–9 Feb)	O_3 – 40.1 (38.9)	Moderate O_3 peak in the afternoon, while moderate CO and NO_X appears during the morning and evening	Moderate wind, low PBLH (~383 m), and low VC (~527 m s^{-1})	Low VC and high CO and NO_X in the evening indicates local source activities
	CO – 526 (333)		RH ≤ 72%, $T \leq 19$ °C, WD = 115 (E)	
	NO_X – 6.4 (6.6)			
IV (26–30 Mar)	O_3 – 45.6 (47.8)	Moderate O_3 in the afternoon, while moderate CO appears in the evening and NO_X in the morning	High wind, moderate PBLH (~849 m), and high VC (~2525 m s^{-1})	Regional O_3 transport, while CO and NO_X levels at night indicate local activities
	CO – 382 (292)		RH ≤ 52%, $T \leq 30$ °C, WD = 122 (E)	
	NO_X – 6.8 (6.5)			
V (11 Apr–20 Apr)	O_3 – 52.2 (51.8)	Moderate peaks of O_3 and CO in the afternoon, while NO_X peaks appear during the night	Moderate wind, PBLH (~930 m), and VC (~1020 m s^{-1})	Afternoon CO level shows local source activities, NO_X dominates at night indicating regional transport
	CO – 526 (464)		RH ≤ 51%, $T \leq 32$ °C, WD = 146 (SE)	
	NO_X – 5.9 (5.1)			
VI (13–20 May)	O_3 – 69.9 (56.3)	High peaks of O_3 in the afternoon, while increasing levels of CO and NO_X appear in the morning	High wind, high PBLH (~1108 m), and high VC (~4639 m s^{-1})	Regional O_3 and elevated peaks of CO at night indicates local source activities
	CO – 547 (413)		RH ≤ 38%, $T \leq 35$ °C, WD = 207 (SW)	
	NO_X – 6.5 (5.8)			
VII (27–30 May)	O_3 – 46.8 (49.5)	Moderate peaks of O_3 and high NO_X in the afternoon, while CO appears in the morning	High wind, moderate PBLH (~900 m), and high VC (~3080 m s^{-1})	Regional transport of O_3 and NO_X, and CO level indicates local source activities
	CO – 509 (413)		RH ≤ 54%, $T \leq 32$ °C, WD = 121 (E)	
	NO_X – 7.5 (6.8)			
VIII (17–18 Oct)	O_3 – 46.9 (53.2)	Moderate O_3 in the afternoon, CO peaks appear before noon and inclined levels of NO_X appear in the early morning	High wind, moderate PBLH (~646 m), and high VC (~3280 m s^{-1})	O_3 level during pre-Diwali due to firecrackers, petty variation of CO before noon indicates fire activities
	CO – 417 (425)		RH ≤ 48%, $T \leq 28$ °C, WD = 152 (SE)	
	NO_X – 4.9 (4.4)			
IX (7–19 Nov)	O_3 – 16.5 (11.7)	Low ozone and an increasing trend of CO and NO_X is observed in the night, morning, and evening	High wind, low PBLH (~500 m), and moderate VC (~1832 m s^{-1})	Regional biomass burning from north IGP
	CO – 1030 (902)		RH ≤ 67%, $T \leq 22$ °C, WD = 177 (S)	
	NO_X – 9.5 (9.1)			
X (2–8 Dec)	O_3 – 19.8 (11.3)	Low ozone and high CO appear in the evening, while NO_X appears in the morning to before noon	High wind, low PBLH (~357 m), and moderate VC (~1280 m s^{-1})	High NO_X indicates long-range transport and CO due to local sources
	CO – 721 (777)		RH ≤ 62%, $T \leq 18$ °C, WD = 223 (W)	
	NO_X – 10.4 (9.6)			
XI (23–30 Dec)	O_3 – 14.7 (10.2)	Low ozone, and high CO appears in the evening and late night, while NO_X appears in the morning to before noon	High wind, low PBLH (~276 m), and moderate VC (~1078 m s^{-1})	High levels of CO and NO_X indicate regional biomass burning
	CO – 1081 (950)		RH ≤ 72%, $T \leq 15$ °C, WD = 217 (SW)	
	NO_X – 8.6 (7.7)			

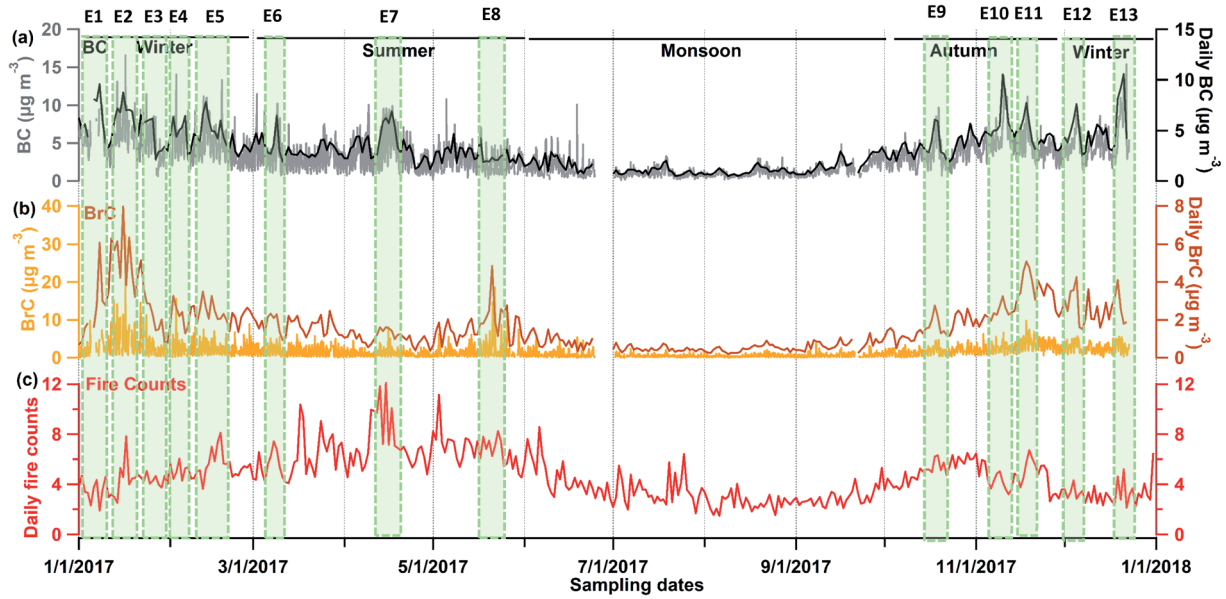

Fig. 2 Hourly and daily variations in BC (top panel) and BrC (middle panel) concentrations, and daily fire counts (bottom panel) over IGP-CARE during the sampling period (January 2017 to December 2017). The light-green shaded areas correspond to episodic events, *i.e.* events during which the concentrations of BC and BrC were at least three times the hourly mean (3 × hourly mean) over the sampling period.

BC.[12,68,69] It is noted that harvesting of rabi and kharif crops in India begins in April–May and mid-October to mid-November months, therefore we can also expect that residue burning in April–May.[51] The BC and BrC levels in episode E8 and diel patterns were different from the previous episodes (Fig. 2 and S3† in the ESI). There was moderate association between BrC and fire radiative power (FRP) for episode E8 (Fig. S5† in the ESI). Nevertheless, when we carefully examined the double peaks of the BrC/BC ratio during the day from 20 May to 21 May 2017, we found that BrC and BC were correlated strongly ($0.23 < r^2 < 0.77$, see Tables 2 and S4† in the ESI) and BrC and CO were also correlated well ($0.87 < r^2 < 0.97$, see Table S5† in the ESI). The appearance of these double peaks at odd times in the diel pattern of E8, *e.g.* midnight and early morning, is an indicator of a special local event of burning with smoldering of moist biomass. Such events are likely during summers in rural Bundelkhand when farmers fire their mud bricks using dung cakes and wood covered in wet mud to protect the fire/prevent heat leaks from pits containing mud bricks. Smoldering in such firing is initially high and can be characterized by high BrC and BC well correlated with CO as observed during E8 (Table S5† in the ESI).

Episode E9 coincided with the Diwali festival when large amounts of fireworks are let off. During the festival, both anthropogenic regional emissions and local emission sources generally display unusual patterns.[70–72] As shown in Fig. 2, this episode was characterized by high BC (6.5 μg m^{-3}) and low BrC (2.4 μg m^{-3}) concentrations with low fire counts. It should also be noted that BC concentrations were strongly associated with BrC (correlation coefficient: $0.81 < r^2 < 0.89$, see Table S4† in the ESI), while CO showed moderate to high association with BC and BrC for this event (see Table S5† in the ESI). Therefore, it is suggested that BC, BrC, and CO had similar origins. During this episode, the RH was moderate (58%), the VC was high, and BC levels peaked in the morning, suggesting a strong contribution from regional-scale firework displays combined with local biomass burning (Table 2).

Episode E10 was characterized by high BC (9.5 μg m^{-3}) and low BrC (2.9 μg m^{-3}) levels, low fire counts, and a low BrC/BC ratio (Fig. 2 and Table 2). The poor association between BC and BrC ($0.13 < r^2 < 0.26$, Table S4† in the ESI) indicates that BC and BrC originate from mixed sources or regional-scale biomass burning events in the northern IGP. Afternoon high BC levels and high dispersion indicate regional biomass burning in the northern IGP and plausible contributions from long-distance urban sources (time series of SLCP concentrations in Fig. S7† in the ESI). In contrast, during episodes E11 and E12, BC values were moderate, and the BrC/BC ratio was rather high (Fig. 2 and Table 2). Moderate levels of BC and BrC and high BrC/BC indicate local moist biomass with smoldering type burning as BC and BrC were well correlated (E11: $0.56 < r^2 < 0.89$; E12: $0.37 < r^2 < 0.89$) during the event days. In episode E13, the BC value was higher (see Fig. 2 and Table 2) than in the other winter episodes. In addition, BC and BrC were weakly correlated (see Fig. S4† in the ESI), indicating that they originated from different and mixed sources. SLCP levels peaked at night and in the evening, indicating a major contribution from mixed local sources such as biomass cookstoves and fires for heating.

Overall, episodic events of elevated BC and BrC concentrations can be attributed to the local biomass burning activities in the neighboring rural communities. Therefore, it is suggested that high concentrations of BrC were mostly primary in nature and thought to be co-emitted with BC from biomass burning activities. However, the above results showed that the observed episodic events are complex and influenced by several factors including sources and meteorological conditions as well as

interlinked atmospheric processes such as dilution and dispersion of pollutants, condensation–evaporation of organic species due to interlinked thermodynamics, heterogeneous chemical reactions, and photochemical processes. Therefore, a comprehensive analysis of molecular characterization of BrC is imperative and it will be investigated in our companion paper using high-resolution time of flight chemical ionization mass spectrometry (HR-ToF-CIMS).

3.4 Temporal variation of O_3, CO, and NO_X

Eleven episodic events (I–XI) in the hourly concentrations of O_3, CO, and NO_X were identified; these events are highlighted using yellow shading in Fig. 3 and are briefly summarized in Table 3. These events (I–XI) were identified using the same criterion (an hourly mean target pollutant concentration of at least 3 times the hourly mean over the entire study period) as used to identify episodic SLCP events (see Table S3† in the ESI). It is noted that CO and NO_X datasets were missing during July to September 2017 due to power interruptions, equipment malfunctions, and system failures at the site. Therefore, there will be limited discussion of the missing data.

The episodic event I was characterized by low O_3 (35.0 ppbv) levels with high levels of CO (636.0 ppbv) and NO_X (9.6 ppbv). The CO concentrations were weakly associated with NO_X, indicating that they probably originated from mixed emission sources. However, the low VC and the fact that CO and NO_X levels peaked during the morning and evening (see Fig S8† in the ESI) suggest slow dispersion of pollutants with a dominant contribution from local biomass burning sources. The combination of low average O_3 levels with high CO and NO_X can be explained by the low solar radiation during the episode. Like episode I, episodic event II was characterized by low levels of O_3 (~27.4 μg m^{-3}), high CO (1041.0 μg m^{-3}), and high NO_X (9.3). During this episode, O_3 and NO_X levels peaked in the afternoon (when the VC was low), while CO levels were highest in the evening. The afternoon O_3 peaks can be attributed to photochemical processes in the presence of high CO and other co-emitted pollutant precursors (not measured in this study) and NO_X levels (see Fig S8† in the ESI). During events III and IV, O_3 levels were higher than during events I and II, while CO and NO_X abundance was low (Fig. 3 and Table 3). Strong diurnal variations combined with a high VC indicate that regional transport was an important source of O_3, while the relatively high CO and NO_X levels at night can be attributed to local biomass burning activities (see Fig. S8†). The summer events (V to VII) had high O_3 levels (46.8–69.9 ppbv), and lower CO and NO_X concentrations than winter events (Fig. 3). The moderate to high wind and VC and low RH (38–51%) probably suppressed secondary formation during these episodes, and the abundances of CO and NO_X were high during the morning and afternoon (see Fig S8† in the ESI). These findings indicate a strong contribution from regional O_3 transport within the IGP together with contributions from local sources near the IGP-CARE site. Event VIII coincided with Diwali when emissions varied due to firework displays and sporadic regional transport of SLCPs.[70–72] As shown in Fig. 2, this episode was characterized by high O_3 levels (46.9 ppbv). The diel patterns of high CO and NO_X during the morning (see Fig S8† in the ESI) indicate contributions from local and regional fire activities. The high O_3 level during episode VIII can be explained by a strong contribution from photochemical processes in the presence of high NO_X and CO levels. The CO and NO_X were correlated and suggest that they

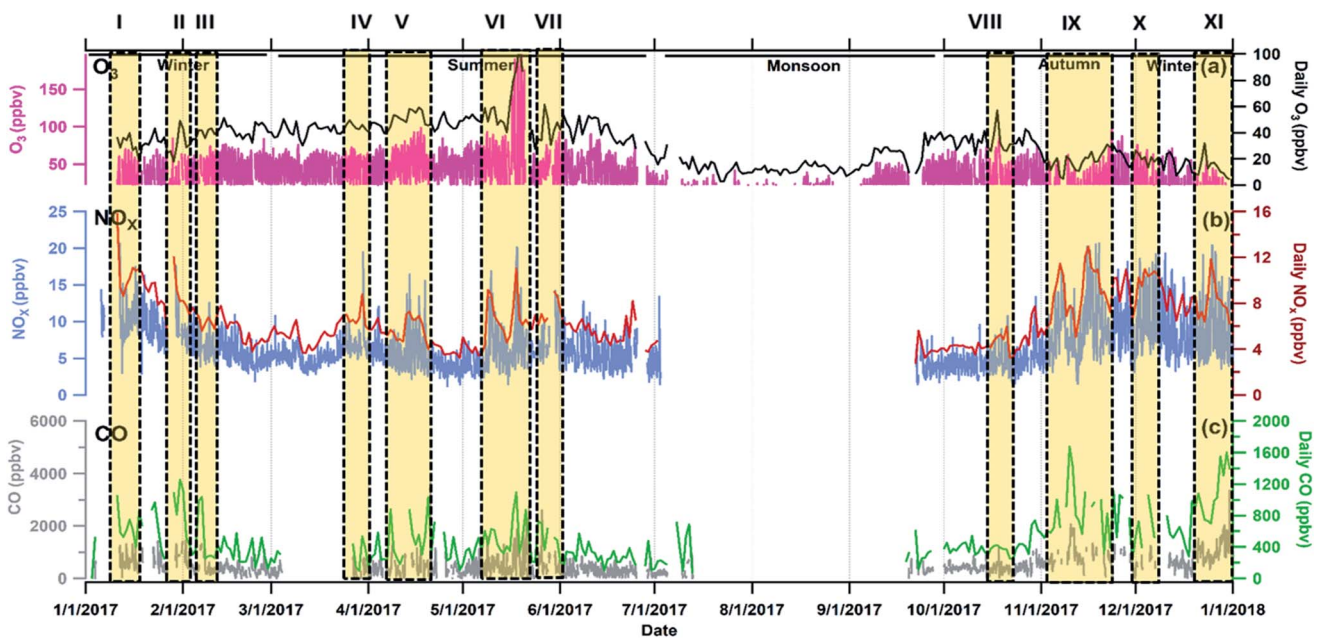

Fig. 3 Hourly and daily variations of O_3 (top panel), NO_X (middle panel), and CO (bottom panel) concentrations over the IGP-CARE site during the sampling period (January 2017 to December 2017). The light-yellow shaded areas correspond to episodic events, *i.e.* events during which the concentrations of the measured pollutants were at least three times the hourly mean (3 × hourly mean) O_3, CO and NO_X concentrations over the sampling period.

probably were co-emitted from the local biomass burning. Other co-pollutants of BC, BrC, CO, and NO_X are the unidentified semi-volatile and volatile organic compounds (VOCs) from the local biomass burning. It must be noted that the site is far away from the fossil fuel combustion influences and only regional transport is thought to occasionally affect the site, hence the obvious source for these pollutants is local biomass burning. The biomass burning, therefore, is a key source of VOCs that are thought to be participating in the photochemical processes during the daytime to contribute to the formation of ozone locally.

Episode IX featured low O_3 levels (16.5 ppbv), high CO (1030.0 ppbv), and NO_X (9.5 ppbv) (Fig. 3 and Table 3), with moderate RH (67%) and high VC. During this event, CO levels peaked at night while NO_X peaked in the morning (see Fig. S4†). The low average O_3 levels suggest a minimal contribution from photochemical reactions of local biomass burning emissions together with an influx of air masses from the northern IGP region plausibly containing titrated O_3 combined with high CO and NO_X. Episodic events X and XI were also characterized by low O_3 levels combined with high CO and NO_X and were likely to be linked to the transport of regional air pollution to the IGP-CARE site.

Overall, the observed O_3 levels were formed locally through photochemical processes and the chemistry of precursors from local biomass burning. However, on a few unusual occasions, O_3 was also thought to be transported to the site from urban areas during the summertime through regional transport. These results show that the observed episodic events are complex and influenced by several factors including aerosol sources and meteorological conditions as well as interlinked atmospheric processes. It is thus clear that meteorological factors strongly affect the temporal distributions of the SLCPs at the studied rural site in the IGP, as well as secondary formation, accumulation from primary sources, and SLCP transportation.

3.5 Seasonal variation of SLCPs

The diurnal profiles of BC, BrC, BrC/BC ratio, and NO_X/BC ratio in different seasons are shown in Fig. 4a–d (left panel). In winter, BC and BrC concentrations had a bimodal diurnal distribution with concentrations peaking in the early morning (6.0 and 4.0 μg m^{-3} for BC and BrC) and night (6.5 and 4.4 μg m^{-3} for BC and BrC, respectively) and being the lowest during the daytime (4.2 and 1.8 μg m^{-3}). The *t*-test indicated that the BC concentration in the mornings in winter was significantly higher ($p < 0.05$) than in other seasons. The low VC and calm winds during winter suggest that the regularly observed high peaks of BC and BrC in the mornings and evenings can be attributed to local biomass burning for cooking and heating. During morning hours (6:00–8:00 AM), low PBLH and VC, limited solar radiation, low temperature, and low wind speeds all favored substantial increases in BC concentrations, as shown in Fig. 4a. During the evening and late at night, BrC concentrations increased gradually due to the low VC and low temperature, especially in winter and autumn seasons. However, the morning and early night peaks were less prominent during the monsoon season than in other seasons due to the wash-out effect (Fig. 4b). The diurnal variation of BC and BrC from other studies was similar to the present study.[45,73]

The BrC/BC ratio is an indicator of biomass burning and other fossil fuel combustion sources, as well as secondary aerosol formation.[61–64] A low BrC/BC ratio in combination with higher NO_X to BC ratio indicates fossil fuel combustion,[74] *e.g.* diesel vehicles (11–47) and gasoline vehicles (1940–4407), while a high BrC/BC ratio suggests the dominance of biomass burning with low NO_X to BC ratio (0.9–2.5).[75] This is because high temperature in the fossil fuel combustion system emits relatively high NO_X and low BrC. In light of all this, an interesting diurnal variation of the BrC/BC ratio was also observed at IGP-CARE. The humps of the BrC/BC ratio in the morning and evening in all seasons were clearly observed (see Fig. 4c). These humps were not associated with the NO_X/BC ratio, while there were similar CO humps in the mornings in all seasons (see Fig. 4d and 5b). This suggests that BrC, BC, and CO were co-emitted from local biomass burning from cooking and/or heating activities. Further, the BrC/BC ratio decreased sharply during daylight hours and increased at night (see Fig. 4c). The BrC/BC ratio was higher in winter and autumn than in summer and the monsoon season. This can partially be attributed to more BrC partitioning to the gas phase, photobleaching, and interlinked atmospheric chemistry during the latter two seasons.

Box plots of the seasonal BC, BrC, BrC/BC ratio, and NO_X/BC ratio are shown in Fig. 4e–g. The 'boxes' indicate the 25th and 75th percentile values, while the solid red and black lines indicate the mean and median (50th percentile) values and the black dots indicate the 5th and 95th percentile outliers of the BC and BrC concentrations and the BrC/BC ratio. The median concentrations of BC and BrC fell between winter and summer, reached a minimum during the monsoon, and then increased in autumn (Fig. 4d and e). The highest BC concentration was observed in winter (5.5 ± 2.0 μg m^{-3}, median = 4.6 μg m^{-3}), followed by autumn (4.1 ± 1.9 μg m^{-3}, median = 3.8 μg m^{-3}), summer (2.8 ± 1.8 μg m^{-3}, median = 2.4 μg m^{-3}), and monsoon (1.2 ± 0.7 μg m^{-3}, median = 1.0 μg m^{-3}). A similar pattern was observed for the BrC concentration.

As noted above, a high BrC/BC ratio suggests a dominant contribution of biomass burning while a low ratio may indicate a plausible contribution from fossil fuel combustion. Several publications have also suggested that BrC may be a precursor of secondary organic aerosols (SOA).[12,19,76] The BrC/BC ratio in winter did not differ significantly ($p > 0.05$) from that in autumn but was significantly higher than that observed in the summer and monsoon seasons. Similarly, NO_X/BC ratios were not significantly different in winter (1.8) and autumn seasons (1.8), while the NO_X/BC ratio was higher in summer (2.4) and monsoon (4.5) (see Fig. 4h). In general, these ratios are significantly lower than those observed for fossil fuels,[74] and comparable with NO_X to BC ratios from forest fires.[75] These findings substantiate our interpretation that the main sources for the observed BC and BrC levels were biomass burning near the site; however, the seasonal similarities and variability can be attributed to biomass material and burning complexities and meteorological factors prevailing during various seasons.

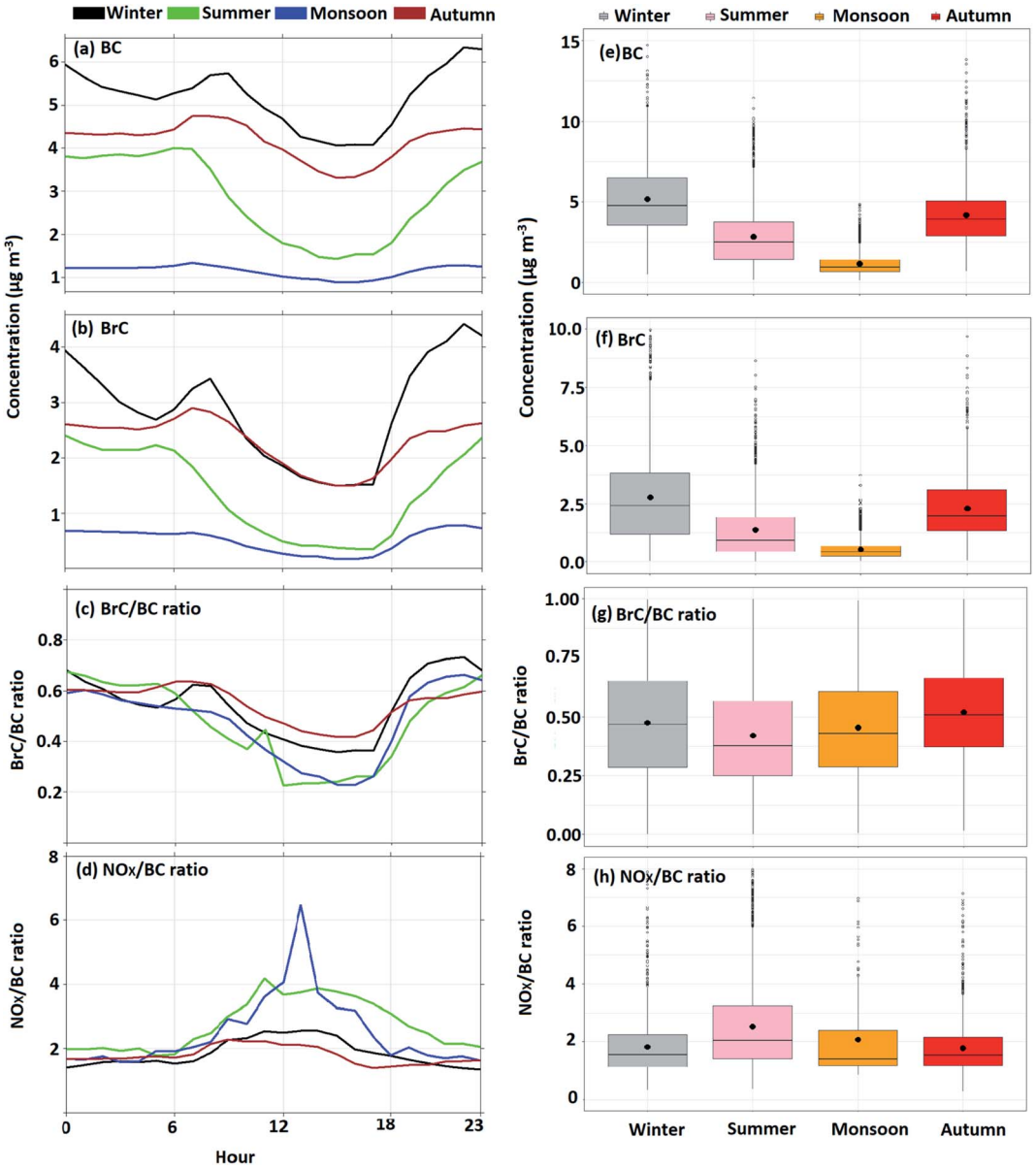

Fig. 4 (a–d) Diurnal variations of BC, BrC, BrC/BC ratio, and NO_X/BC ratio in four seasons at the IGP-CARE site during the 2017 sampling period. The black, green, blue, and brown lines show results for the winter, summer, monsoon, and autumn seasons. (e–h) Box plots of seasonal concentrations of BC, BrC, BrC/BC ratio, and NO_X/BC ratio. The 'boxes' indicate the 25th and 75th percentile values, while the black circles and black lines indicate mean and median values.

The diurnal variations of O_3, CO, and NO_X at IGP-CARE during the winter, summer, monsoon, and autumn seasons are shown in Fig. 5a–c. In all seasons, the O_3 concentration peaked during the day (1100–1600 PM) and typically declined after 17:00 IST. During summer, the lowest observed O_3 level was 22 ppbv (hourly average) and its maximum was 66 ppbv. The lowest O_3 concentrations occurred in the monsoon season when the O_3 concentration ranged from 25 ppbv to as low as 10 ppbv at night (Fig. 5a). During winter, the day-time peak concentrations of O_3 reached 52 ppbv and the night-time concentration was as low as ~10 ppbv, which is similar to the monsoon season O_3 level despite the different meteorology and concentrations in the two seasons. This may be because the availability of relatively high amounts of NO_2 during the day-time[3] enables O_3 production by oxidation of hydroxyl (OH) radicals and trace gases such as CO and CH_4, whereas O_3 is destroyed in the absence of solar radiation at night, leading to the slow conversion of NO to NO_2.

The observed diurnal O_3 patterns were compared to those for a typical urban city, namely Delhi (see Fig. S9† in the ESI) in the year 2014. Two distinct diurnal patterns were observed in Delhi,[33,77] both of which differed slightly from those seen at IGP-CARE, especially in the morning and afternoon. The rate of change of O_3 ($d(O_3)/dt$) in the morning hours (08:00–11:00 AM) and evening hours (17:00–19:00 PM) at IGP-CARE and other sites in India is summarized in Table S6† of the ESI, where it is

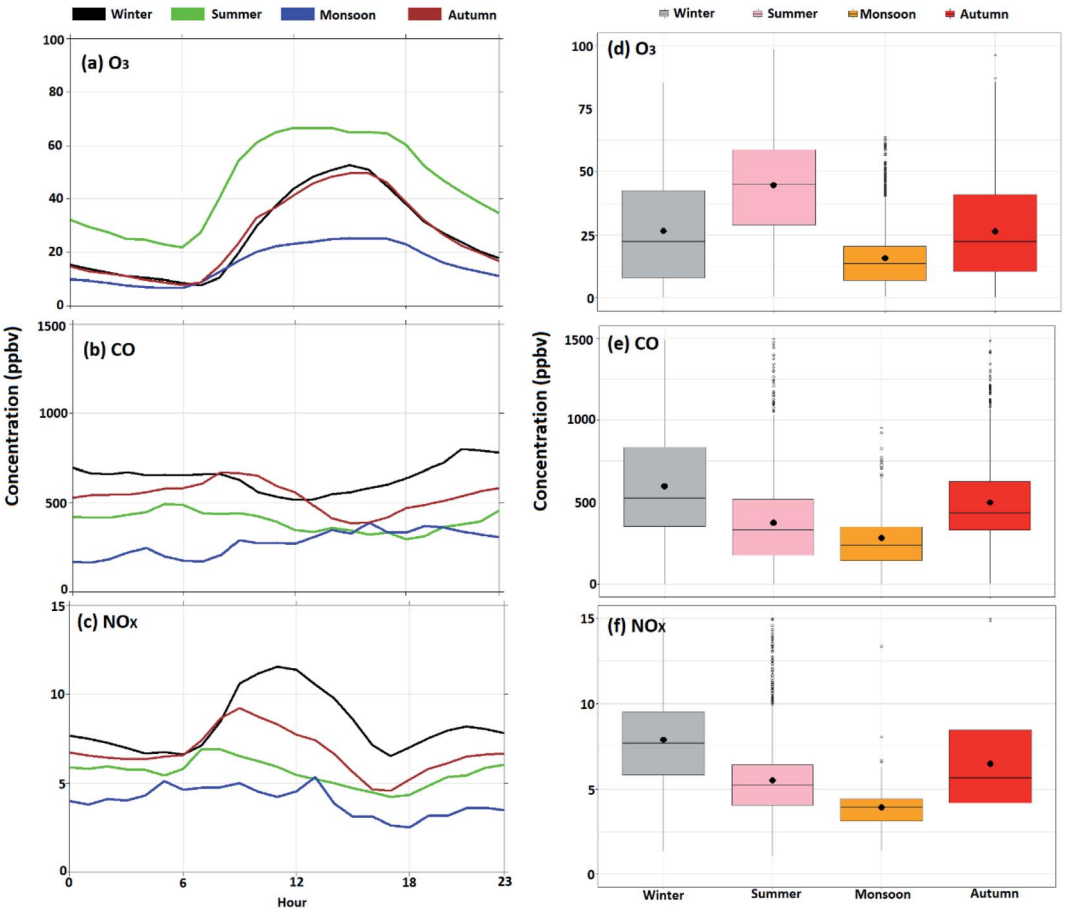

Fig. 5 (a–c) Diurnal variations in hourly O_3, CO, and NO_X concentrations during four seasons at the IGP-CARE site during the 2017 sampling period. The black, green, blue, and brown lines show results for the winter, summer, monsoon, and autumn seasons, and grey lines indicate standard deviations in seasons. (d–f) Box plots of seasonal O_3, CO, and NO_X concentrations. The 'boxes' indicate the 25th and 75th percentile values, while the black circles and black lines indicate mean and median values.

normalized against the reported VC values for each site. The average rate of change of O_3 in the morning at the rural IGP-CARE site was 6.8 ppbv h^{-1} which is close to that seen at the semi-urban site[78] at Mohali (7.3 ppbv h^{-1}) and 39% higher than that at the urban site of Delhi. These differences suggest a slow production of O_3 from trace gas precursors or a strong influence from the NO titration effect in Delhi. The average rate of change of O_3 during the evening at IGP-CARE (-5.3 ppbv h^{-1}) is close to that seen at the semi-urban Mohali site. The rate of change in the O_3 concentration in the morning at IGP-CARE was higher than at other sites including Gadanki, Anantapur, Ahmedabad, Thumba, Joharpur, and Tranquebar. This may indicate that NO_X production at rural sites is lower than in urban and sub-urban regions, and implies that titration effects were minimal at the IGP-CARE site. Seasonal rates of change in the O_3 concentration were also estimated (see Table S6† in the ESI); in the evening hours, the rate of change in the O_3 concentration was highest in the autumn, followed by winter, summer, and monsoon.

Generally, the CO concentration at IGP-CARE had a bimodal and unsymmetrical diurnal profile (Fig. 5b). Its concentration was high in the morning during winter, possibly because of extensive biomass combustion in cooking stoves. Later in the day, rising atmospheric temperatures led to increased dilution (*i.e.*, high VC) and dispersion, causing CO concentrations to fall. High CO concentrations were observed at night in winter (738 ± 33 ppbv), probably because of incomplete combustion of biomass fuel (wood, straw, and cow dung cakes) for cooking and heating.[69] During summer and monsoon, daytime and night-time CO concentrations did not differ significantly ($p > 0.05$). This can be due to high dilutions due to higher VC during the summer and significant washout of pollutants during the monsoon season. NO_X concentrations were generally higher during the day-time (0800–1500 IST; 8.0–10.0 ppbv), especially in the winter and autumn. The NO_2 concentration was highest in winter (8.5 ± 3.2 ppbv) and autumn (7.1 ± 3.4 ppbv) due to anthropogenic activity (Fig. S10† in the ESI). As the sun rises (07:00–09:00 IST), photochemical reactions begin, and NO is rapidly oxidized into NO_2 in the presence of O_3. The fact that NO_2 concentrations were higher than NO concentrations during this period demonstrates the strong influence of local sources near IGP-CARE. The average NO_2/NO_X ratio over the sampling period was 0.93 ± 0.05, indicating extensive conversion of NO to NO_2 at the site. Previous studies[79,80] have also reported NO_2/NO_X

ratios in the range of 0.81–0.90 at a rural site and attributed them to high NO to NO_2 conversion. Conversely, Mazzeo *et al.*[81] measured the urban NO_2/NO_X ratio in the range of 0.02–0.05, which they attributed to vehicular emissions. The higher NO_2/NO_X ratios observed in the present study indicate that the influence of vehicle sources at the IGP-CARE site was minimal. Both the NO_X and CO showed reasonably good agreement in their concentration profiles, and this indicates that they were plausibly co-emitted from the biomass burning activities in nearby rural communities. The emissions from forest fires reported by Mieville *et al.* (2010)[75] showed CO/NO_X ratio in the range between 18 and 70. In this study, the CO/NO_X ratio was higher (mean value 83 ± 47) than that observed for forest fires. These values are way higher than those observed from fossil fuel combustion sources elsewhere (*e.g.* the CO/NO_2 ratio ranged between 5 and 50).[82] Therefore, the measured higher CO/NO_X ratio in this study confirms that CO and NO_X were co-emitted from the local biomass burning activities.

Box plots of the seasonal O_3, CO, and NO_X levels are presented in Fig. 5d–f. The O_3 concentration was highest in summer (46 ppbv), while those of CO (498 and 604 ppbv in autumn and winter) and NO_X (6.6 and 7.9 ppbv) were highest in winter and autumn, respectively. Overall, secondary pollutant tropospheric O_3 showed elevated concentration. O_3 peaks were mostly attributed to local ozone formation. Nevertheless, on several occasions, O_3 emission was also attributed to regional urban areas.

3.6 Brown carbon (BrC) and interlinked chemistry

In general, the BrC time series indicates that BrC, BC, CO, and NO_X followed similar patterns in various seasons. This suggests that BrC was co-emitted with BC from the local biomass burning for cooking and heating needs. Thus, mostly the measured BrC in this study was primary in nature, which is hypothesized to be transformed significantly during the day-time. The profile of the BrC/BC ratio evolved astonishingly during the day-time. An extremely sharp decline in the BrC/BC ratio at the time of dawn each morning indicates the dominance of photochemical processes in the transformation of BrC. This transformation of BrC was observed to decrease the attenuation of light absorption at 375 nm in this study. The decrease in the ability to absorb light by organic aerosols in reference to BrC was termed bleaching. To investigate the "bleaching" of brown carbon, we analyzed the variability of BrC, BC, and O_3 levels during the daytime and the night-time at IGP-CARE as functions of temperature and solar radiation. BrC bleaching reduced the BrC/BC ratio, as shown in Fig. 4c, and was strong during the daytime. Recent studies have suggested that strongly light-absorbing primary BrC (BrC_{pri}) may rapidly evolve into weakly light-absorbing secondary BrC (BrC_{sec}) in the atmosphere; this process is known as BrC "bleaching".[83] As shown in Fig. S11† of the ESI, BrC levels correlated strongly with the O_3 concentration and the spatially averaged temperature, whereas BC levels correlated only weakly with the O_3 concentration. Several factors could potentially explain the day-time decrease in the BrC/BC ratio, including photochemical processes (which would be consistent with the sharp decrease in the BrC/BC ratio during the early morning hours), radical chemistry (*i.e.* reactions with OH and/or O_3) and the volatilization of BrC compounds at elevated temperatures during the midday hours. Interestingly, temperature correlated better with BrC/BC during the daytime than at night. Further experiments are planned to investigate the relative contributions of the above-mentioned factors, and the roles of photochemistry and radical chemistry in "brown carbon bleaching" will be investigated in a companion paper using HR-ToF-CIMS.

3.7 Influence of meteorology on SLCPs at IGP-CARE

In addition to atmospheric chemistry and atmospheric processes, meteorological factors also influenced the concentrations and properties of SLCPs. Therefore, local and regional source locations were investigated using local meteorological data and air-mass back trajectories. As noted in the preceding section, levels of SLCFs at IGP-CARE were generally higher in winter and autumn than in other seasons. Fig. 6 shows CBPF plots for SLCPs (BC, BrC, CO, NO_X, and CO) in winter (top panel) and autumn (bottom panel). In both seasons, high CBPF values for BC were observed when the wind speed was <2 m s^{-1} and the local wind was northerly. The highest CBPF values for BrC were associated with moderate to high wind speeds (2–10 m s^{-1}) from the northwestern and western directions in winter and autumn (Fig. 6). It must be noted that the site is surrounded from all directions by the rural communities located within 2–10 km, which largely burn biomass for their daily needs of cooking and heating throughout the year. Therefore, most distinct morning and evening peaks of BC, BrC, CO, and NO_X observed round the year are thought to be from local biomass burning for cooking and heating needs (see Fig. S12† in the ESI).

Similar patterns are visible in the CBPF plots for O_3 and NO_X in both seasons (Fig. 6, top and bottom panels). This indicates that moderate to high wind speeds favor regional transportation of BrC, O_3, and NO_X.[84] Conversely, the high CBPF values for CO associated with low wind speeds (<2 m s^{-1}) in the northwestern and western directions can be attributed to local sources that are active in both seasons. CBPF plots for the studied SLCPs in the summer and monsoon seasons are presented in Fig. S13† of the ESI. A similar pattern was observed for BC and CO in both seasons, with high CBPF values being associated with moderate wind speeds (2–4 m s^{-1}) from the northern and northeastern directions. In contrast to BC, BrC, and CO, the CBPF plots of O_3 and NO_X somehow exhibited different patterns in the summer and monsoon seasons. Overall, the CBPF plots of BC, BrC, and CO reveal a clear dominance of local emission sources, whereas regional transport appears to be important for O_3 and NO_X.

To understand the impact of regional sources on SLCPs at IGP-CARE, we performed a cluster analysis on a group of air mass back trajectories with similar origins. Four major contributing clusters (C1, C2, C3, and C4) were identified based on total spatial variance (TSV) using a variance threshold of 20% as recommended by Sateesh *et al.*[85] (2018) for different seasons

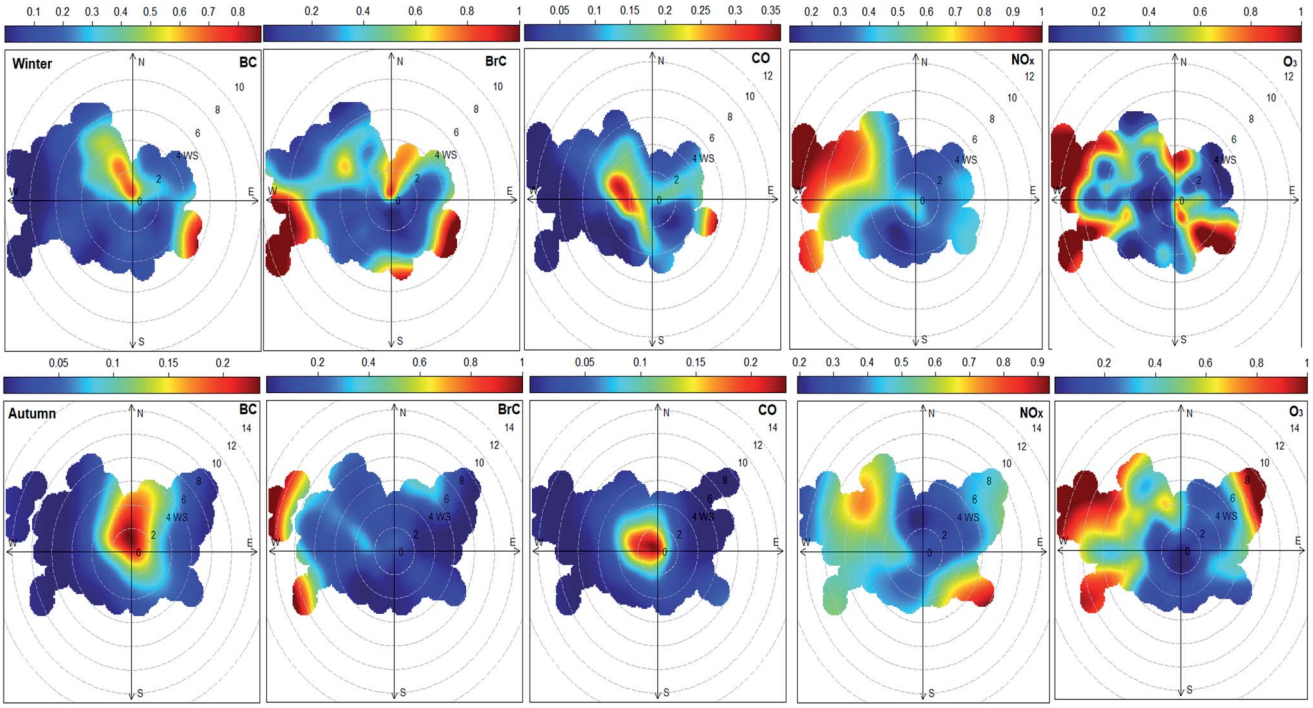

Fig. 6 CBPF plots of SLCPs in winter (top panel) and autumn (bottom panel) over IGP-CARE during 2017. The chosen threshold was the 75th percentile of the measured SLCP concentrations.

(see Fig. S14† of the ESI and the discussion in Text S3† of the ESI). Overall, the cluster analysis explained a significant fraction of the seasonal variability in local and regional/super-regional air masses and clarified the relative importance of regional and interannual sources by quantifying the differences between the clusters in terms of SLCP concentrations. However, such analyses cannot be used to determine the contributions of potential source regions at the receptor site; for this purpose, a PSCF analysis was used to apportion the relevant back trajectories with species concentrations at the receptor site. PSCF plots for the studied SLCPs are presented in Fig. 7. The color scale used in each of these maps indicates PSCF probabilities measuring the likelihood of different source origins for each species measured at the receptor site. A threshold criterion corresponding to the 75th percentile of SLCP concentrations was used to identify specific sources.

For BC and BrC, the PSCF analysis identified regional sources in the northwestern "hot spot" region of the IGP, which encompasses Delhi, Punjab, Haryana, and northern Pakistan. These sources were especially important in winter and autumn. Some eastern parts of Uttar Pradesh were also important regional BC sources in autumn, presumably because of industrial activity near Kanpur (Fig. 7, left top panel). It should be noted that the highest BC and BrC levels were associated with low winds and sources local to the receptor region, which cannot be detected using the PSCF. For O_3, the highest PSCF (>0.8) values occurred during summer days and were linked to a potential source in the north-western IGP. In other seasons, a few hotspots (0.4–0.6) were identified in the north-western and eastern regions of Uttar Pradesh. In the monsoon season and winter, the PSCF map of O_3 was dominated by local emissions (Fig. 7, right top panel), while regional sources dominated during summer and autumn. A probable origin location for CO emissions was identified in a small region of Uttar Pradesh, which was a particularly prominent source in autumn (Fig. 7, left bottom panel). The PSCF map for NO_X highlighted north-eastern Delhi, Punjab, Haryana, and northern Pakistan (Fig. 7, right bottom panel). Overall, the PSCF analysis indicates that the SLCPs detected at IGP-CARE mainly originated from local sources but that the contributions from regional emission sources in the northwestern IGP region cannot be ruled out on some occasions.

3.8 Comparison with previous studies

The annual mean concentrations of pollutants including BC, O_3, CO, and NO_X measured in the present study are summarized in Table 4 and compared with average values reported from other cities of the world. In comparison, the present BC levels were higher by a factor of 5–12 from USA[86–88] and UK,[89] while being close to values reported in Chen *et al.* (2017),[90] Putero *et al.* (2015),[18] and Cao *et al.* (2006)[91] for Asian cities (Beijing, Hong Kong, and Kathmandu). Recent studies reported that the emissions of BC from Asia (China and India) are substantially high;[4,92] however, predominant sources of BC in these countries are diverse. BC emission in India is mostly from residential biomass fuel and open biomass burning,[93] while in China, the BC emission is largely from industrial and residential biomass fuel.[94] In urban cities, on-road transport (combustion of diesel, gasoline, and CNG vehicles) is the major contributor in India.[95,96] It should be noted that the BC level observed in the

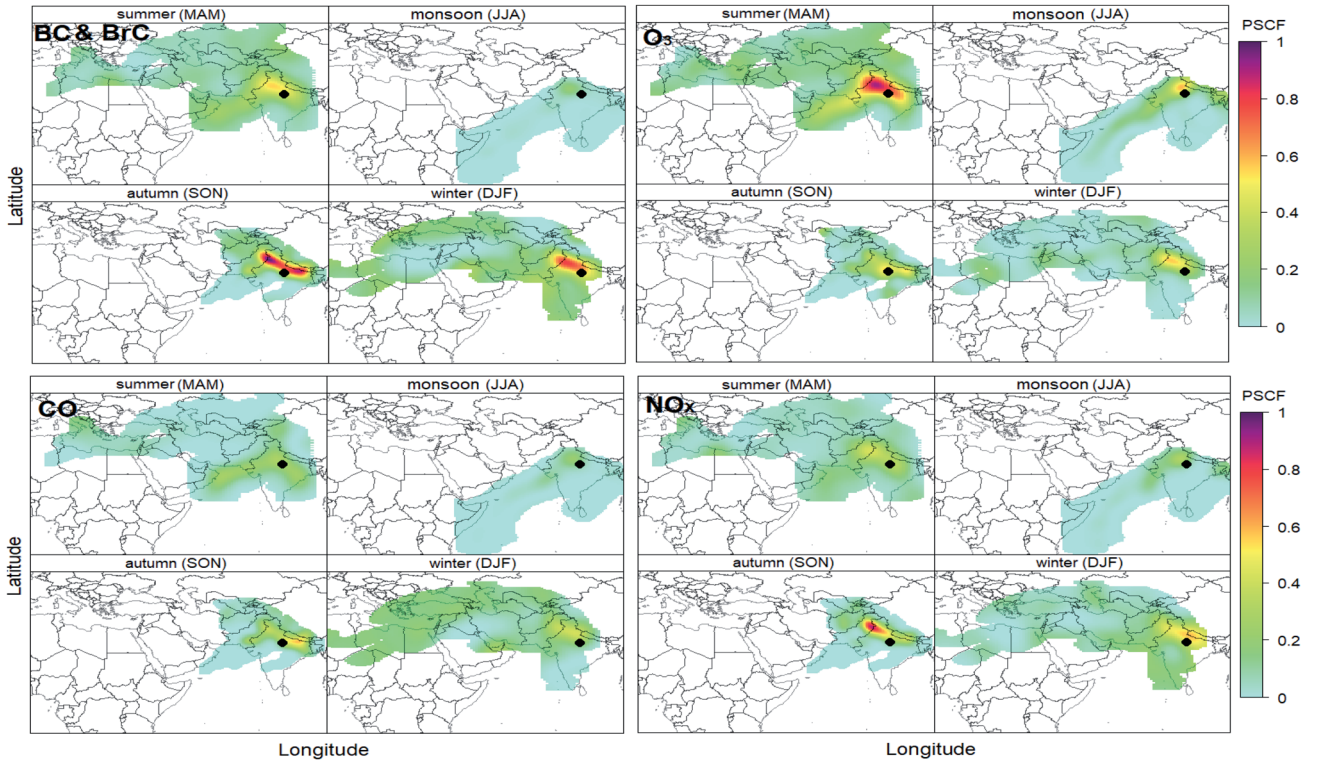

Fig. 7 PSCF plots of SLCP concentrations based on 4 day air mass back-trajectories over the IGP-CARE site at the 500 m ABL. The black circle indicates the location of IGP-CARE (the receptor site in a rural part of the IGP region). The threshold criterion corresponded to the 50th percentile of the measured SLCP concentrations.

present study was lower compared to the values reported for Delhi (10.3 ± 5.4), Agra (12.4 ± 4.3), Kanpur (8.6 ± 4.1) and Banaras, respectively.[45,58] The BrC concentration (2.6 ± 1.3 μg m^{-3}) in the present work was also lower compared to the value reported for Banaras (6.0 ± 3.7 μg m^{-3}).[45] It is also noted that the average BC in the present study was higher by a factor of 2 from rural sites (Anantapur).[58]

The annual mean of O_3 at IGP-CARE was close to those in Los Angeles,[86] Kathmandu,[18] and Indian cities such as Delhi,[38] Agra,[97] and Kanpur.[98] Interestingly, the present concentration of O_3 was found to be 1.5–3.0 times higher compared to values

Table 4 The key SLCPs measured at IGP-CARE and comparison with other cities all over the world[a]

Location	Site type	BC[b]	BrC[b]	O_3[c]	NO_X[c]	CO[c]
New York	U	0.7 ± 0.2[d]		10.3 ± 3.6[d]	—	—
Los Angeles	U	1.6 ± 0.4[e]		27.1 ± 11.5[f]	46.6 ± 31.4[f]	530 ± 300[f]
London	U	1.3 ± 1.0[g]		11.0[h]	54.1[h]	398.5[h]
Beijing	U	9.4 ± 6.3[i]		20.0[j]	30.0[j]	741.6[j]
Hong Kong	U	13.6[k]		18.7[k]	27.7[l]	—
Kathmandu	U	11.6 ± 10.7[m]		27.0 ± 21.3[m]	—	603 ± 204[n]
New Delhi	U	10.3 ± 5.4[o]		25.0 ± 10.2[p]	30.5 ± 8.5[p]	1970[p]
Agra	U	12.4 ± 4.3[o]		32.3 ± 22.7[q]	12.3 ± 2.5[q]	477 ± 392[q]
Kanpur	U	8.6 ± 4.1[o]		27.9 ± 17.8[r]	5.7 ± 4.5[r]	721 ± 403[r]
Banaras	U	11.8 ± 8.6[s]	6.0 ± 3.7[s]			
Anantapur	R	2.7 ± 0.7[o]		40.7 ± 3.7[t]	5.1 ± 0.7[t]	436 ± 64[u]
Present study	**R**	**5.1 ± 2.2**	**2.6 ± 1.3**	**31.4 ± 23.1**	**8.6 ± 3.5**	**659 ± 437**

[a] Abbreviations – U: urban, R: rural. [b] Values are reported in μg m^{-3}. [c] Values are reported in ppbv. [d] Value averaged from Venkatachari *et al.* (2006).[88] [e] Average BC mass concentrations were summarized from the US EPA (2012).[87] [f] Average values of O_3, NO_X, and CO reported in Delfino *et al.* (2011).[86] [g] From Reche *et al.* (2011).[89] [h] Average values of O_3, NO_X, and CO reported in Reche *et al.* (2011).[89] [i] Average values of BC were compiled in Chen *et al.* (2017).[90] [j] From Stohl *et al.* (2015).[99] [k] Average BC concentration reported in Cao *et al.* (2006).[91] [l] From Sun *et al.* (2019).[101] [m] From Putero *et al.* (2015).[18] [n] Average values of CO compiled from Bhardwaj *et al.* (2017).[102] [o] Average values of BC for Indian cities were compiled from Rana *et al.* (2019).[58] [p] From Tiwari *et al.* (2015).[38] [q] From Verma *et al.* (2017).[97] [r] From Gaur *et al.* (2014).[98] [s] From Srivastava *et al.* (2019).[45] [t] From Reddy *et al.* (2012).[100] [u] From Ahammed *et al.* (2006).[103]

reported in New York,[88] London,[89] Beijing,[99] and Hong Kong.[91] A high mean O_3 was observed at Anantapur (40.7 ± 3.7 ppbv, rural site)[97,100] compared to the present study, possibly due to photochemical processes involving the precursors in the presence of solar radiation. The annual average of NO_X at IGP-CARE (8.6 ± 3.5 ppbv) is generally lower than the values reported from New York,[88] Los Angeles,[86] London[89] and other Asian cities,[99,101] while the average CO emission (659 ± 437 ppbv) level was higher compared to the values reported for Los Angeles,[86] London,[89] and Kathmandu.[102] Interestingly, the levels of NO_X and CO in New Delhi[38] and China[99] were considerably higher than in the present study. The level of NO_X and CO at Anantapur,[100,103] were lower than the value reported in the present work.

4. Conclusions

We have presented one-year (January 2017 to December 2017) long measurements of key SLCPs, *i.e.* BC, BrC, and O_3, and other important gases along with meteorological data gathered at the rural IGP-CARE site. These measurements were used to investigate the variation in SLCP concentrations at IGP-CARE as well as the atmospheric transformations of these pollutants and their sources at the studied site. Thirteen episodic events (E1–E13) of elevated BC and BrC concentrations were characterized. The elevated concentrations of BC and BrC observed can be attributed to the local biomass burning (wood, agricultural residues, and dung cakes) for cooking and heating by the surrounding rural neighborhoods. The high concentrations of BrC observed are suggested to be primary in nature and thought to be co-emitted with BC from biomass burning. Also, episodic events of high O_3 concentrations were characterized. These O_3 peaks can be attributed to local ozone formation. Nevertheless, on several occasions, higher O_3 levels can also be attributed to regional transport from urban areas. The BrC/BC ratio decreased sharply during daylight hours (08:00–17:00 IST) and slowly increased at night (18:00–23:00 IST), especially in the winter and autumn; this may have been associated with BrC bleaching, which is thought to be affected by temperature, solar radiation, and ozone/radical chemistry. CBPF plots suggested that strong BC contributions from the north-west and the north in winter (Jan., Feb., and Dec. 2017) and autumn (Sep., Oct., and Nov. 2017) were associated with lower wind speeds and low VC, while trajectory cluster and PSCF analysis revealed a seasonal variation in SLCP sources. It is likely that regional sources affected the local SLCP concentrations at the IGP-CARE. The high concentrations and temporal distributions of SLCPs can partly explain local and regional scales at the IGP-CARE site in winter and autumn using PSCF analysis. In contrast, in the summer and monsoon seasons, strong convection (unstable atmospheric conditions) likely favored the dilution of pollutants. Future studies should focus on long-term monitoring of SLCPs and modeling the atmospheric processes and heterogeneous uptakes and their chemistry. The knowledge generated through such investigations could guide the development of effective mitigation strategies for managing climate change while ensuring food security and protecting human health.

Author contributions

JP: methodology, software, validation, writing – original draft, and writing – review & editing; HRM: monitoring, data curation, analysis, and writing – review and editing; KM: data curation, analysis, and writing – review and editing; BC: monitoring, data curation, and analysis; MH: review & editing; GH: writing – review & editing; GT: review & editing; JBCP: review & editing; JB: review & editing; HP: review & editing; RKP: supervision, conceptualization, project administration, funding acquisition, methodology, writing – review & editing, and correspondence.

Conflicts of interest

All authors declare that they have no known competing financial interests or any personal relationships that could have appeared to influence the work reported in this research paper.

Acknowledgments

This project is funded by The Swedish Research Council, Vetenskaprådet (VR) under the U-Forsk Grant (dr No. 348-2014-3496). We are grateful to The Swedish Research Council, Vetenskaprådet (VR), Sweden.

References

1 K. R. Smith, M. Jerrett, H. R. Anderson, R. T. Burnett, V. Stone, R. Derwent, R. W. Atkinson, A. Cohen, S. B. Shonkoff, D. Krewski, C. A. Pope, M. J. Thun and G. Thurston, Public health benefits of strategies to reduce greenhouse-gas emissions: health implications of short-lived greenhouse pollutants, *Lancet*, 2009, **374**, 2091–2103.
2 IGSD, *Primer on Short-Lived Climate Pollutants*, 2013.
3 J. H. Seinfield and S. N. Pandis, *Atmospheric Chemistry and Physics: From Air Pollution to Climate Change*, John Willey & Sons. Inc, New York, vol. 51, 2006.
4 T. C. Bond, S. J. Doherty, D. W. Fahey, P. M. Forster, T. Berntsen, B. J. Deangelo, M. G. Flanner, S. Ghan, B. Kärcher, D. Koch, S. Kinne, Y. Kondo, P. K. Quinn, M. C. Sarofim, M. G. Schultz, M. Schulz, C. Venkataraman, H. Zhang, S. Zhang, N. Bellouin, S. K. Guttikunda, P. K. Hopke, M. Z. Jacobson, J. W. Kaiser, Z. Klimont, U. Lohmann, J. P. Schwarz, D. Shindell, T. Storelvmo, S. G. Warren and C. S. Zender, Bounding the role of black carbon in the climate system: A scientific assessment, *J. Geophys. Res.: Atmos.*, 2013, **118**, 5380–5552.
5 IPCC, *IPCC Fifth Assessment Report: Climate Change 2013*, 2013.
6 Z. Zhao, J. Cao, J. C. Chow, J. G. Watson, A. L. W. Chen, X. Wang, Q. Wang, J. Tian, Z. Shen, C. Zhu, S. Liu, J. Tao, Z. Ye, T. Zhang, J. Zhou and R. Tian, Multi-wavelength light absorption of black and brown carbon at a high-

altitude site on the Southeastern margin of the Tibetan Plateau, China, *Atmos. Environ.*, 2019, **212**, 54–64.

7 Q. Wang, Y. Han, J. Ye, S. Liu, S. Pongpiachan, N. Zhang, Y. Han, J. Tian, C. Wu, X. Long, Q. Zhang, W. Zhang, Z. Zhao and J. Cao, High Contribution of Secondary Brown Carbon to Aerosol Light Absorption in the Southeastern Margin of Tibetan Plateau, *Geophys. Res. Lett.*, 2019, **46**, 4962–4970.

8 Q. Wang, J. Ye, Y. Wang, T. Zhang, W. Ran, Y. Wu, J. Tian, L. Li, Y. Zhou, S. S. Hang Ho, B. Dang, Q. Zhang, R. Zhang, Y. Chen, C. Zhu and J. Cao, Wintertime Optical Properties of Primary and Secondary Brown Carbon at a Regional Site in the North China Plain, *Environ. Sci. Technol.*, 2019, **53**, 12389–12397.

9 D. G. Kaskaoutis, G. Grivas, C. Theodosi, M. Tsagkaraki, D. Paraskevopoulou, I. Stavroulas, E. Liakakou, A. Gkikas, N. Hatzianastassiou, C. Wu, E. Gerasopoulos and N. Mihalopoulos, Carbonaceous aerosols in contrasting atmospheric environments in Greek cities: Evaluation of the EC-tracer methods for secondary organic carbon estimation, *Atmosphere*, 2020, **11**, 4.

10 UNEP and WMO, *Integrated Assessment of Black Carbon and Tropospheric Ozone*, 2011.

11 UNEP, *HFCs: A Critical Link in Protecting Climate and the Ozone Layer*, 2011.

12 B. Srinivas and M. M. Sarin, Brown carbon in atmospheric outflow from the Indo-Gangetic Plain: Mass absorption efficiency and temporal variability, *Atmos. Environ.*, 2014, **89**, 835–843.

13 B. Srinivas and M. M. Sarin, Light absorbing organic aerosols (brown carbon) over the tropical Indian Ocean: impact of biomass burning emissions, *Environ. Res. Lett.*, 2013, **8**, 044042.

14 S. C. Anenberg, J. Schwartz, D. Shindell, M. Amann, G. Faluvegi, Z. Klimont, G. Janssens-Maenhout, L. Pozzoli, R. Van Dingenen, E. Vignati, L. Emberson, N. Z. Muller, J. J. West, M. Williams, V. Demkine, W. K. Hicks, J. Kuylenstierna, F. Raes and V. Ramanathan, Global Air Quality and Health Co-benefits of Mitigating Near-Term Climate Change through Methane and Black Carbon Emission Controls, *Environ. Health Perspect.*, 2012, **120**, 831–839.

15 N. A. H. Janssen, G. Hoek, M. Simic-Lawson, P. Fischer, L. van Bree, H. ten Brink, M. Keuken, R. W. Atkinson, H. R. Anderson, B. Brunekreef and F. R. Cassee, Black Carbon as an Additional Indicator of the Adverse Health Effects of Airborne Particles Compared with PM10 and PM2.5, *Environ. Health Perspect.*, 2011, **119**, 1691–1699.

16 D. Shindell, J. C. I. Kuylenstierna, E. Vignati, R. van Dingenen, M. Amann, Z. Klimont, S. C. Anenberg, N. Muller, G. Janssens-Maenhout, F. Raes, J. Schwartz, G. Faluvegi, L. Pozzoli, K. Kupiainen, L. Höglund-Isaksson, L. Emberson, D. Streets, V. Ramanathan, K. Hicks, N. T. K. Oanh, G. Milly, M. Williams, V. Demkine and D. Fowler, Simultaneously Mitigating Near-Term Climate Change and Improving Human Health and Food Security, *Science*, 2012, **335**, 183–189.

17 P. S. Monks, A. T. Archibald, A. Colette, O. Cooper, M. Coyle, R. Derwent, D. Fowler, C. Granier, K. S. Law, G. E. Mills, D. S. Stevenson, O. Tarasova, V. Thouret, E. von Schneidemesser, R. Sommariva, O. Wild and M. L. Williams, Tropospheric ozone and its precursors from the urban to the global scale from air quality to short-lived climate forcer, *Atmos. Chem. Phys.*, 2015, **15**, 8889–8973.

18 D. Putero, P. Cristofanelli, A. Marinoni, B. Adhikary, R. Duchi, S. D. Shrestha, G. P. Verza, T. C. Landi, F. Calzolari, M. Busetto, G. Agrillo, F. Biancofiore, P. Di Carlo, A. K. Panday, M. Rupakheti and P. Bonasoni, Seasonal variation of ozone and black carbon observed at Paknajol, an urban site in the Kathmandu Valley, Nepal, *Atmos. Chem. Phys.*, 2015, **15**, 13957–13971.

19 M. Hallquist, J. C. Wenger, U. Baltensperger, Y. Rudich, D. Simpson, M. Claeys, J. Dommen, N. M. Donahue, C. George, A. H. Goldstein, J. F. Hamilton, H. Herrmann, T. Hoffmann, Y. Iinuma, M. Jang, M. E. Jenkin, J. L. Jimenez, A. Kiendler-Scharr, W. Maenhaut, G. McFiggans, T. F. Mentel, A. Monod, A. S. H. Prévôt, J. H. Seinfeld, J. D. Surratt, R. Szmigielski and J. Wildt, The formation, properties and impact of secondary organic aerosol: current and emerging issues, *Atmos. Chem. Phys.*, 2009, **9**, 5155–5236.

20 J. Lelieveld, P. J. Crutzen, V. Ramanathan, M. O. Andreae, C. A. M. Brenninkmeijer, T. Campos, G. R. Cass, R. R. Dickerson, H. Fischer, J. A. de Gouw, A. Hansel, A. Jefferson, D. Kley, A. T. J. de Laat, S. Lal, M. G. Lawrence, J. M. Lobert, O. L. Mayol-Bracero, A. P. Mitra, T. Novakov, S. J. Oltmans, K. A. Prather, T. Reiner, H. Rodhe, H. A. Scheeren, D. Sikka and J. Williams, Pollution from South and Southeast Asia The Indian Ocean Experiment : Widespread Air Pollution from South and Southeast Asia, *Science*, 2001, **291**, 1031–1036.

21 A. Laskin, J. Laskin and S. A. Nizkorodov, *Chem. Rev.*, 2015, **115**, 4335–4382.

22 P. K. Aggarwal, P. K. Joshi, J. S. I. Ingram and R. K. Gupta, Adapting food systems of the Indo-Gangetic plains to global environmental change: key information needs to improve policy formulation, *Environ. Sci. Policy*, 2004, **7**, 487–498.

23 V. Ramanathan and G. Carmichael, Global and regional climate changes due to black carbon, *Nat. Geosci.*, 2008, **1**, 221–227.

24 M. R. Olson, M. V. Garcia, M. A. Robinson, P. Van Rooy, M. A. Dietenberger, M. Bergin and J. J. Schauer, Investigation of black and brown carbon multiple-wavelength- dependent light absorption from biomass and fossil fuel combustion source emissions, *J. Geophys. Res.: Atmos.*, 2015, 6682–6697.

25 T. Saud, D. P. Singh, T. K. Mandal, R. Gadi, H. Pathak, M. Saxena, S. K. Sharma, R. Gautam, A. Mukherjee and R. P. Bhatnagar, Spatial distribution of biomass consumption as energy in rural areas of the Indo-Gangetic plain, *Biomass Bioenergy*, 2011, **35**, 932–941.

26 P. Sadavarte and C. Venkataraman, Trends in multi-pollutant emissions from a technology-linked inventory for India: I. Industry and transport sectors, *Atmos. Environ.*, 2014, **99**, 353–364.
27 K. Tibrewal and C. Venkataraman, COVID-19 lockdown closures of emissions sources in India: Lessons for air quality and climate policy, *J. Environ. Manage.*, 2022, **302**, 114079.
28 V. Ramanathan, M. V. Ramana, G. Roberts, D. Kim, C. Corrigan, C. Chung and D. Winker, Warming trends in Asia amplified by brown cloud solar absorption, *Nature*, 2007, **448**, 575–578.
29 V. Ramanathan and Y. Feng, Air pollution, greenhouse gases and climate change: Global and regional perspectives, *Atmos. Environ.*, 2009, **43**, 37–50.
30 O. Gustafsson, M. Kruså, Z. Zencak, R. J. Sheesley, L. Granat, E. Engström, P. S. Praveen, P. S. P. Rao, C. Leck and H. Rodhe, Brown clouds over South Asia: biomass or fossil fuel combustion?, *Science*, 2009, **323**, 495–498.
31 U. C. C. Dumka, D. G. G. Kaskaoutis, S. Tiwari, P. D. D. Safai, S. D. D. Attri, V. K. K. Soni, N. Singh and N. Mihalopoulos, Assessment of biomass burning and fossil fuel contribution to black carbon concentrations in Delhi during winter, *Atmos. Environ.*, 2018, **194**, 93–109.
32 B. Sinha, K. Singh Sangwan, Y. Maurya, V. Kumar, C. Sarkar, B. P. Chandra and V. Sinha, Assessment of crop yield losses in Punjab and Haryana using 2 years of continuous in situ ozone measurements, *Atmos. Chem. Phys.*, 2015, **15**, 9555–9576.
33 S. Tyagi, S. Tiwari, A. Mishra, P. K. Hopke, S. D. Attri, A. K. Srivastava and D. S. Bisht, Spatial variability of concentrations of gaseous pollutants across the National Capital Region of Delhi, India, *Atmos. Pollut. Res.*, 2016, **7**, 808–816.
34 S. Ramachandran, M. Rupakheti and M. G. Lawrence, *Environ. Int.*, 2020, 142.
35 P. Cristofanelli, D. Putero, B. Adhikary, T. C. Landi, A. Marinoni, R. Duchi, F. Calzolari, P. Laj, P. Stocchi, G. Verza, E. Vuillermoz, S. Kang, J. Ming and P. Bonasoni, Transport of short-lived climate forcers/pollutants (SLCF/P) to the Himalayas during the South Asian summer monsoon onset, *Environ. Res. Lett.*, 2014, **9**, 084005.
36 K. Ram, M. M. Sarin and P. Hegde, Long-term record of aerosol optical properties and chemical composition from a high-altitude site (Manora Peak) in Central Himalaya, *Atmos. Chem. Phys.*, 2010, **10**, 11791–11803.
37 T. Sarangi, M. Naja, N. Ojha, R. Kumar, S. Lal, S. Venkataramani, A. Kumar, R. Sagar and H. C. Chandola, First simultaneous measurements of ozone, CO, and NOy at a high-altitude regional representative site in the central Himalayas, *J. Geophys. Res.: Atmos.*, 2014, **119**, 1592–1611.
38 S. Tiwari, A. Dahiya and N. Kumar, Investigation into relationships among NO, NO2, NOx, O3, and CO at an urban background site in Delhi, India, *Atmos. Res.*, 2015, **157**, 119–126.
39 B. Srinivas and M. M. Sarin, Brown carbon in atmospheric outflow from the Indo-Gangetic Plain: Mass absorption efficiency and temporal variability, *Atmos. Environ.*, 2014, **89**, 835–843.
40 R. Satish, P. Shamjad, N. Thamban, S. Tripathi and N. Rastogi, Temporal Characteristics of Brown Carbon over the Central Indo-Gangetic Plain, *Environ. Sci. Technol.*, 2017, **51**, 6765–6772.
41 S. Tiwari, A. Dahiya and N. Kumar, *Atmos. Res.*, 2015, **157**, 119–126.
42 U. C. Dumka, K. K. Moorthy, S. N. Tripathi, P. Hegde and R. Sagar, Altitude variation of aerosol properties over the Himalayan range inferred from spatial measurements, *J. Atmos. Sol.-Terr. Phys.*, 2011, **73**, 1747–1761.
43 X. Pei, M. Hallquist, A. C. Eriksson, J. Pagels, N. M. Donahue, T. Mentel, B. Svenningsson, W. Brune and R. K. Pathak, Morphological transformation of soot: Investigation of microphysical processes during the condensation of sulfuric acid and limonene ozonolysis product vapors, *Atmos. Chem. Phys.*, 2018, **18**, 9845–9860.
44 D. A. Lack, J. M. Langridge, R. Bahreini, C. D. Cappa, A. M. Middlebrook and J. P. Schwarz, Brown carbon and internal mixing in biomass burning particles, *Proc. Natl. Acad. Sci. U. S. A.*, 2012, **109**, 14802–14807.
45 S. Srivastava, M. Kumar, R. S. Singh, B. N. Rai, R. K. Mall and T. Banerjee, Long-term observation of black carbon aerosols at an urban location over the central Indo-Gangetic Plain, South Asia, *Atmósfera*, 2019, **32**, 95–113.
46 L. Caponi, P. Formenti, D. Massabó, C. Di Biagio, M. Cazaunau, E. Pangui, S. Chevaillier, G. Landrot, M. Andreae, K. Kandler, S. Piketh, T. Saeed, D. Seibert, E. Williams, Y. Balkanski, P. Prati and J.-F. Doussin, Spectral- and size-resolved mass absorption efficiency of mineral dust aerosols in the shortwave: a simulation chamber study, *Atmos. Chem. Phys.*, 2017, 1–39.
47 T. Rathod, S. K. Sahu, M. Tiwari, A. Yousaf, R. C. Bhangare and G. G. Pandit, Light absorbing properties of brown carbon generated from pyrolytic combustion of household biofuels, *Aerosol Air Qual. Res.*, 2017, **17**, 108–116.
48 H. E. Redmond, K. D. Dial and J. E. Thompson, Light scattering and absorption by wind blown dust: Theory, measurement, and recent data, *Aeolian Res.*, 2010, **2**, 5–26.
49 H. A. Jafar and R. M. Harrison, Spatial and temporal trends in carbonaceous aerosols in the United Kingdom, *Atmos. Pollut. Res.*, 2021, **12**(1), 295–305.
50 D. Butterfield, S. Beccaceci, P. Quincey, B. Sweeney, A. Lillley, C. Bradshaw, G. Fuller, D. Green and A. Font, *2015 Annual Report for the UK Black Carbon Network*, 2016.
51 D. P. Dee, S. M. Uppala, A. J. Simmons, P. Berrisford, P. Poli, S. Kobayashi, U. Andrae, M. A. Balmaseda, G. Balsamo, P. Bauer, P. Bechtold, A. C. M. Beljaars, L. van de Berg, J. Bidlot, N. Bormann, C. Delsol, R. Dragani, M. Fuentes, A. J. Geer, L. Haimberger, S. B. Healy, H. Hersbach, E. V. Hólm, L. Isaksen, P. Kållberg, M. Köhler, M. Matricardi, A. P. Mcnally, B. M. Monge-Sanz, J. J. Morcrette, B. K. Park, C. Peubey, P. de Rosnay, C. Tavolato, J. N. Thépaut and F. Vitart, The ERA-Interim

reanalysis: Configuration and performance of the data assimilation system, *Q. J. R. Meteorol. Soc.*, 2011, **137**, 553–597.

52 A. Virkkula, T. Mäkelä, R. Hillamo, T. Yli-Tuomi, A. Hirsikko, K. Hämeri and I. K. Koponen, A simple procedure for correcting loading effects of aethalometer data, *J. Air Waste Manage. Assoc.*, 2007, **57**, 1214–1222.

53 I. Ježek, L. Drinovec, L. Ferrero, M. Carriero and G. Močnik, Determination of car on-road black carbon and particle number emission factors and comparison between mobile and stationary measurements, *Atmos. Meas. Tech.*, 2015, **8**, 43–55.

54 A. Petzold, J. A. Ogren, M. Fiebig, P. Laj, S.-M. Li, U. Baltensperger, T. Holzer-Popp, S. Kinne, G. Pappalardo, N. Sugimoto, C. Wehrli, A. Wiedensohler and X.-Y. Zhang, Recommendations for reporting "black carbon" measurements, *Atmos. Chem. Phys.*, 2013, **13**, 8365–8379.

55 E. Weingartner, H. Saathoff, M. Schnaiter, N. Streit, B. Bitnar and U. Baltensperger, Absorption of light by soot particles: Determination of the absorption coefficient by means of aethalometers, *J. Aerosol Sci.*, 2003, **34**, 1445–1463.

56 M. Collaud Coen, E. Weingartner, A. Apituley, D. Ceburnis, R. Fierz-Schmidhauser, H. Flentje, J. S. Henzing, S. G. Jennings, M. Moerman, A. Petzold, O. Schmid and U. Baltensperger, Minimizing light absorption measurement artifacts of the Aethalometer: Evaluation of five correction algorithms, *Atmos. Meas. Tech.*, 2010, **3**, 457–474.

57 J. H. Kim, S. W. Kim, J. A. Ogren, P. J. Sheridan, S. C. Yoon, S. Sharma and N. H. Lin, Multiple scattering correction factor estimation for aethalometer aerosol absorption coefficient measurement, *Aerosol Sci. Technol.*, 2019, **53**, 160–171.

58 A. Rana, S. Jia and S. Sarkar, Black carbon aerosol in India: A comprehensive review of current status and future prospects, *Atmos. Res.*, 2019, **218**, 207–230.

59 D. C. Carslaw and K. Ropkins, Openair – An r package for air quality data analysis, *Environ. Model. Software*, 2012, **27–28**, 52–61.

60 I. Uria-Tellaetxe and D. C. Carslaw, Conditional bivariate probability function for source identification, *Environ. Model. Software*, 2014, **59**, 1–9.

61 O. Bansal, A. Singh and D. Singh, Characteristics of Black Carbon aerosols over Patiala Northwestern part of the IGP: Source apportionment using cluster and CWT analysis, *Atmos. Pollut. Res.*, 2018, **10**, 244–256.

62 E. Liakakou, I. Stavroulas, D. G. Kaskaoutis, G. Grivas, D. Paraskevopoulou, U. C. Dumka, M. Tsagkaraki, A. Bougiatioti, K. Oikonomou, J. Sciare, E. Gerasopoulos and N. Mihalopoulos, Long-term variability, source apportionment and spectral properties of black carbon at an urban background site in Athens, Greece, *Atmos. Environ.*, 2020, **222**, 117137.

63 U. C. Dumka, D. G. Kaskaoutis, P. C. S. Devara, R. Kumar, S. Kumar, S. Tiwari, E. Gerasopoulos and N. Mihalopoulos, Year-long variability of the fossil fuel and wood burning black carbon components at a rural site in southern Delhi outskirts, *Atmos. Res.*, 2019, **216**, 11–25.

64 H. Herich, C. Hueglin and B. Buchmann, A 2.5 year's source apportionment study of black carbon from wood burning and fossil fuel combustion at urban and rural sites in Switzerland, *Atmos. Meas. Tech.*, 2011, **4**, 1409–1420.

65 S. Gani, S. Bhandari, S. Seraj, D. S. Wang, K. Patel, P. Soni, Z. Arub, G. Habib, L. Hildebrandt Ruiz and J. S. Apte, Submicron aerosol composition in the world's most polluted megacity: The Delhi Aerosol Supersite study, *Atmos. Chem. Phys.*, 2019, **19**, 6843–6859.

66 N. M. Donahue, A. L. Robinson, C. O. Stanier and S. N. Pandis, Coupled partitioning, dilution, and chemical aging of semivolatile organics, *Environ. Sci. Technol.*, 2006, **40**, 2635–2643.

67 S. Gani, S. Bhandari, S. Seraj, D. S. Wang, K. Patel, P. Soni, Z. Arub, G. Habib, L. Hildebrandt Ruiz and J. S. Apte, Submicron aerosol composition in the world's most polluted megacity: The Delhi Aerosol Supersite study, *Atmos. Chem. Phys.*, 2019, **19**, 6843–6859.

68 V. Choudhary, G. K. Singh, T. Gupta and D. Paul, Absorption and radiative characteristics of brown carbon aerosols during crop residue burning in the source region of Indo-Gangetic Plain, *Atmos. Res.*, 2021, **249**, 105285.

69 V. Sinha, V. Kumar and C. Sarkar, Chemical composition of pre-monsoon air in the Indo-Gangetic Plain measured using a new air quality facility and PTR-MS: high surface ozone and strong influence of biomass burning, *Atmos. Chem. Phys.*, 2014, **14**, 5921–5941.

70 S. Shivani, R. Gadi, M. Saxena, S. K. Sharma and T. K. Mandal, Short-term degradation of air quality during major firework events in Delhi, India, *Meteorol. Atmos. Phys.*, 2019, **131**, 753–764.

71 K. Patel, S. Bhandari, S. Gani, M. J. Campmier, P. Kumar, G. Habib, J. Apte and L. Hildebrandt Ruiz, Sources and Dynamics of Submicron Aerosol during the Autumn Onset of the Air Pollution Season in Delhi, India, *ACS Earth Space Chem.*, 2021, **5**, 118–128.

72 S. Izhar, P. Rajput and T. Gupta, Variation of particle number and mass concentration and associated mass deposition during Diwali festival, *Urban Clim.*, 2018, 1.

73 S. Tiwari, U. C. Dumka, P. K. Hopke, P. Tunved, A. K. Srivastava, D. S. Bisht and R. K. Chakrabarty, Atmospheric heating due to black carbon aerosol during the summer monsoon period over Ballia: A rural environment over Indo-Gangetic Plain, *Atmos. Res.*, 2016, **178–179**, 393–400.

74 B. Alfoldy, M. M. Mahfouz, A. Gregorič, M. Ivančič, I. Ježek and M. Rigler, Atmospheric concentrations and emission ratios of black carbon and nitrogen oxides in the Arabian/Persian Gulf region, *Atmos. Environ.*, 2021, **256**, 118451.

75 A. Mieville, C. Granier, C. Liousse, B. Guillaume, F. Mouillot, J. F. Lamarque, J. M. Grégoire and G. Pétron, Emissions of gases and particles from biomass burning during the 20th century using satellite data and an

historical reconstruction, *Atmos. Environ.*, 2010, **44**, 1469–1477.
76 S. K. R. Boreddy, K. Kawamura, S. Mkoma and P. Fu, Hygroscopic behavior of water-soluble matter extracted from biomass burning aerosols collected at a rural site in Tanzania, East Africa, *J. Geophys. Res.: Atmos.*, 2014, **119**, 12233–12245.
77 S. Tiwari, D. S. Bisht, A. K. Srivastava and Ö. Gustafsson, Simultaneous measurements of black carbon and PM2.5, CO, and NOx variability at a locally polluted urban location in India, *Nat. Hazards*, 2015, **75**, 813–829.
78 P. Sharma, J. C. Kuniyal, K. Chand, R. P. Guleria, P. P. Dhyani and C. Chauhan, Surface ozone concentration and its behaviour with aerosols in the northwestern Himalaya, India, *Atmos. Environ.*, 2013, **71**, 44–53.
79 S. Han, H. Bian, Y. Feng, A. Liu, X. Li, F. Zeng and X. Zhang, Analysis of the relationship between O3, NO and NO2 in Tianjin, China, *Aerosol Air Qual. Res.*, 2011, **11**, 128–139.
80 D. Pudasainee, B. Sapkota, M. L. Shrestha, A. Kaga, A. Kondo and Y. Inoue, Ground level ozone concentrations and its association with NOx and meteorological parameters in Kathmandu valley, Nepal, *Atmos. Environ.*, 2006, **40**, 8081–8087.
81 N. A. Mazzeo, L. E. Venegas and H. Choren, Analysis of NO, NO2, O3 and NOx concentrations measured at a green area of Buenos Aires City during wintertime, *Atmos. Environ.*, 2005, **39**, 3055–3068.
82 V. P. Aneja, A. Agarwal, P. A. Roelle, S. B. Phillips, Q. Tong, N. Watkins and R. Yablonsky, Measurements and analysis of criteria pollutants in New Delhi, India, *Environ. Int.*, 2001, **27**, 35–42.
83 H. Forrister, J. Liu, E. Scheuer, J. Dibb, L. Ziemba, K. L. Thornhill, B. Anderson, G. Diskin, A. E. Perring, J. P. Schwarz, P. Campuzano-Jost, D. A. Day, B. B. Palm, J. L. Jimenez, A. Nenes and R. J. Weber, Evolution of brown carbon in wildfire plumes, *Geophys. Res. Lett.*, 2015, **42**, 4623–4630.
84 D. S. Bisht, U. C. Dumka, D. G. Kaskaoutis, A. S. Pipal, A. K. Srivastava, V. K. Soni, S. D. Attri, M. Sateesh and S. Tiwari, Carbonaceous aerosols and pollutants over Delhi urban environment: Temporal evolution, source apportionment and radiative forcing, *Sci. Total Environ.*, 2015, **522**, 431–445.
85 M. Sateesh, V. K. Soni, P. V. S. Raju and V. Mor, Cluster analysis of aerosol properties retrieved from a sky-radiometer over a coastal site: Thiruvananthapuram, India, *Atmos. Pollut. Res.*, 2018, **9**, 207–219.
86 R. J. Delfino, N. Staimer and N. D. Vaziri, Air pollution and circulating biomarkers of oxidative stress, *Air Qual., Atmos. Health*, 2011, **4**, 37–52.
87 USEPA, *Report to Congress on Black Carbon*, 2012.
88 P. Venkatachari, L. Zhou, P. Hopke, J. Schwab, K. Demerjian, S. Weimer, O. Hogrefe, D. Felton and O. Rattigan, An intercomparison of measurement methods for carbonaceous aerosol in the ambient air in New York City, *Aerosol Sci. Technol.*, 2006, **40**, 788–795.
89 C. Reche, X. Querol, A. Alastuey, M. Viana, J. Pey, T. Moreno, S. Rodríguez, Y. González, R. Fernández-Camacho, A. M. S. De La Campa, J. De La Rosa, M. Dall'Osto, A. S. H. Prévôt, C. Hueglin, R. M. Harrison and P. Quincey, New considerations for PM, Black Carbon and particle number concentration for air quality monitoring across different European cities, *Atmos. Chem. Phys.*, 2011, **11**, 6207–6227.
90 D. Chen, H. Cui, Y. Zhao, L. Yin, Y. Lu and Q. Wang, A two-year study of carbonaceous aerosols in ambient PM2.5 at a regional background site for western Yangtze River Delta, China, *Atmos. Res.*, 2017, **183**, 351–361.
91 G. Cao, X. Zhang and F. Zheng, Inventory of black carbon and organic carbon emissions from China, *Atmos. Environ.*, 2006, **40**, 6516–6527.
92 A. Rana, S. Jia and S. Sarkar, Black carbon aerosol in India: A comprehensive review of current status and future prospects, *Atmos. Res.*, 2019, **218**, 207–230.
93 A. Pandey, P. Sadavarte, A. B. Rao and C. Venkataraman, Trends in multi-pollutant emissions from a technology-linked inventory for India: II. Residential, agricultural and informal industry sectors, *Atmos. Environ.*, 2014, **99**, 341–352.
94 D. G. Streets, D. T. Shindell, Z. Lu and G. Faluvegi, Radiative forcing due to major aerosol emitting sectors in China and India, *Geophys. Res. Lett.*, 2013, **40**, 4409–4414.
95 J. Prakash and G. Habib, On-road assessment of light duty vehicles in Delhi city: Emission factors of CO, CO2 and NOX, *Atmos. Environ.*, 2018, **174**, 132–139.
96 U. Paliwal, M. Sharma and J. F. Burkhart, Monthly and spatially resolved black carbon emission inventory of India: Uncertainty analysis, *Atmos. Chem. Phys.*, 2016, **16**, 12457–12476.
97 N. Verma, A. Lakhani and K. Maharaj Kumari, High ozone episodes at a semi-urban site in India: Photochemical generation and transport, *Atmos. Res.*, 2017, **197**, 232–243.
98 A. Gaur, S. N. Tripathi, V. P. Kanawade, V. Tare and S. P. Shukla, Four-year measurements of trace gases (SO_2, NO_x, CO, and O_3) at an urban location, Kanpur, in Northern India, *J. Atmos. Chem.*, 2014, **71**, 283–301.
99 A. Stohl, B. Aamaas, M. Amann, L. H. Baker, N. Bellouin, T. K. Berntsen, O. Boucher, R. Cherian, W. Collins, N. Daskalakis, M. Dusinska, S. Eckhardt, J. S. Fuglestvedt, M. Harju, C. Heyes, Ø. Hodnebrog, J. Hao, U. Im, M. Kanakidou, Z. Klimont, K. Kupiainen, K. S. Law, M. T. Lund, R. Maas, C. R. MacIntosh, G. Myhre, S. Myriokefalitakis, D. Olivié, J. Quaas, B. Quennehen, J. C. Raut, S. T. Rumbold, B. H. Samset, M. Schulz, Ø. Seland, K. P. Shine, R. B. Skeie, S. Wang, K. E. Yttri and T. Zhu, Evaluating the climate and air quality impacts of short-lived pollutants, *Atmos. Chem. Phys.*, 2015, **15**, 10529–10566.
100 B. Suresh Kumar Reddy, K. Raghavendra Kumar, G. Balakrishnaiah, K. Rama Gopal, R. R. Reddy, L. S. S. Reddy, Y. Nazeer Ahammed, K. Narasimhulu, K. Krishna Moorthy and S. Suresh Babu, Potential source regions contributing to seasonal variations of black

carbon aerosols over Anantapur in southeast India, *Aerosol Air Qual. Res.*, 2012, **12**, 340–354.

101 S. Sun, L. Tian, W. Cao, P.-C. Lai, P. P. Y. Wong, R. S. Lee, T. G. Mason, A. Krämer and C.-M. Wong, Urban climate modified short-term association of air pollution with pneumonia mortality in Hong Kong, *Sci. Total Environ.*, 2019, **646**, 618–624.

102 P. Bhardwaj, M. Naja, M. Rupakheti, A. K. Panday, R. Kumar, K. Mahata, S. Lal, H. C. Chandola and M. G. Lawrence, Variations in surface ozone and carbon monoxide in the Kathmandu Valley and surrounding broader regions during SusKat-ABC field campaign: role of local and regional sources, *Atmos. Chem. Phys. Discuss.*, 2017, 1–49.

103 Y. N. Ahammed, R. R. Reddy, K. R. Gopal, K. Narasimhulu, D. B. Basha, L. S. S. Reddy and T. V. R. Rao, Seasonal variation of the surface ozone and its precursor gases during 2001-2003, measured at Anantapur (14.62°N), a semi-arid site in India, *Atmos. Res.*, 2006, **80**, 151–164.